Natural Hazards (2024) 120:9609–9647
https://doi.org/10.1007/s11069-024-06579-0

ORIGINAL PAPER

Real-time urban flood modeling: exploring the sub-grid approach for accurate simulation and hazard analysis

R. Reshma[1] · N. Nithila Devi[1] · Soumendra Nath Kuiry[2]

Received: 14 June 2023 / Accepted: 18 March 2024 / Published online: 21 April 2024

Abstract
The increasing magnitude of monetary and life losses caused by urban floods worldwide has sparked a deeper interest among researchers in comprehending these phenomena. Accurate modeling and forecasting of floods play a pivotal role in developing effective strategies for flood damage mitigation and management, thereby reducing associated hazards. A critical concern in this endeavor is optimizing the trade-off between computation time and accuracy when simulating real-time flood events. This paper aims to establish the superiority of the sub-grid approach in achieving accurate simulation results of real-time flood events within minimal computational time. By conducting simulations of one experimental test and two real-world flood events using the HEC-RAS flow simulation model, we demonstrate that the sub-grid approach significantly reduces computation time by approximately 90% while faithfully capturing the dynamics of urban flood. In contrast, the non-sub-grid approach often over-predicts flow dynamics in urban areas and fails to effectively trace building footprints, resulting in unrealistic flow patterns and under or overstating the hazard maps. In a nutshell, the sub-grid hydraulic modeling approach enables better hazard analysis and mapping. The outcomes of this research provide valuable guidance to modelers and authorities, suggesting the adoption of the sub-grid approach for accurate and reliable real-time urban flood modeling, inundation forecasting, and hazard zoning in the context of urban flood hazard analysis.

Keywords Urban flood · Urban flood modeling · Sub-grid approach · Hazard analysis · Flood risk · Hazard map

✉ Soumendra Nath Kuiry
snkuiry@civil.iitm.ac.in

R. Reshma
reshmaradhakrishnan094@gmail.com

N. Nithila Devi
nithiladevi.n@gmail.com

[1] Research Scholar, Department of Civil Engineering, Indian Institute of Technology Madras, Chennai, India

[2] Department of Civil Engineering, Indian Institute of Technology Madras, Chennai, India

1 Introduction

Among all the natural disasters, floods are the most hazardous ones - in terms of severity imposed, life and economic losses incurred, and damages caused. According to global statistics, financial losses incurred due to urban floods surmount those due to other natural disasters such as earthquakes, drought, wildfires, etc. (*EM-DAT | The International Disasters Database*, 2023). Though human interventions cannot completely prevent the occurrence of urban floods, the severity caused and the damages incurred can be significantly reduced through the proper implementation of disaster and flood risk management measures (structural and non-structural). Structural measures involve but are not limited to (i) construction of tidal barriers, embankments, levees, etc., (ii) widening and restoration of water bodies and estuaries, (iii) providing evacuation shelters, etc., while non-structural measures comprise (i) development of codes and practices concerning land use, construction, urbanization, and industrialization, (ii) flood forecasting and emergency action planning, (iii) flood inundation and hazard mapping, etc. (UNDRR 2009). Among these, flood inundation, hazard, and risk mapping are the first and foremost flood management measures (Mohanty et al. 2020). In order to generate these maps, urban flooding can be simulated using different numerical models and software packages available.

The available hydraulic models for flood simulations can be classified into one-dimensional (1D) (Brett and Sanders 2001; Glaister 1988; Testa et al. 2007a), two-dimensional (2D) (Beffa and Connell 2001; *HEC-RAS River Analysis System Hydraulic Reference Manual*, 2016), and three-dimensional (3D) models (Li et al. 2006). Among these, 3D models, which numerically solve the Navier-Stokes equations, are the most accurate. Nevertheless, they are computationally very intensive for simulating a large-scale urban flood. On the other hand, the computationally efficient 1D models may not accurately simulate the flow over the flood plains since they solve the Saint-Venant equation only along the river flow direction. Loss of accuracy in using 1D models is due to the fact that the flood plains in urban areas have complex connectivity and flow patterns due to the presence of several smaller terrain features such as buildings, streets, highways, etc. On the contrary, 2D models based on the solution of the depth-averaged shallow water equations can predict floods by bridging the trade-off in accuracy between 1D and 3D models. The 2D models are recommended for accurate and realistic representation and generation of urban flood flow dynamics (Shustikova et al. 2019). Numerous software packages (commercial and open-source) that use 2D mathematical models are currently available for urban flood modeling – MIKE (https://www.mikepoweredbydhi.com), HEC-RAS (https://www.hec.usace.army.mil/software/hec-ras/documentation.aspx), FLO-2D (https://flo-2d.com/), Flood Modeller (formerly known as ISIS, https://www.floodmodeller.com/), Itzï (Courty et al. 2017), LISFLOOD (Bates and De Roo 2000), and Tuflow (https://www.tuflow.com/) are a few to list. However, the major challenges in adopting the above-cited models are their requirement for reliable and accurate high-resolution urban terrain data and accurate representation of the same in the model setup. The high-resolution Digital Elevation Models (DEM) are, therefore, an essential component for full 2D simulations of urban flood events (Mignot et al. 2019; Mignot and Dewals 2022; Muhadi et al. 2020; Muthusamy et al. 2021; Neal et al. 2009). A coarser DEM may overpredict flood extents while underpredicting the flow depths over the urban floodplains (Muthusamy et al. 2021). Advancements in technology to capture highly accurate topographical details of an urban setting have increased the availability of

high-resolution DEMs to the research community. However, the use of such DEMs adds up the required simulation time due to the requirement of representing the small topographical features, such as buildings, roads, etc., in urban flood modeling. Thus, the usage of 2D models demands computational cost optimization, especially in the case of urban flood modeling and real-time forecasting frameworks. The urban flood modelers have been trying to minimize the overall computational time without sacrificing much accuracy. This has necessitated the development of both software (e.g., model algorithms) and hardware (e.g., multi-core processing) acceleration techniques.

The most commonly adopted methods to reduce computational time are parallelization, machine learning (ML), simplified hydraulic model approach, and the use of either adaptive or sub-grid mesh techniques. The parallelization technique uses Graphical Processing Units (GPU) for performing simulations through parallel computation steps incorporating multiple processors at a time. This method enables the modelers to use high-resolution DEMs with finer topographic data of larger areas of consideration without much expense of computational time (Fernández-Pato and García-Navarro 2021; Neal et al. 2010; Xing et al. 2019). However, the GPU-based flood models are not so popular among practicing engineers and disaster management authorities due to their inherent model complexity and requirements of hardware with high-end configuration. The ML approach utilizes algorithms such as Artificial Neural Networks (ANN), K-nearest neighbor, etc., coupled with existing hydraulic models to increase the computational speed of the hybrid ML models (Hosseiny et al. 2020; Hou et al. 2021; Kwon and Kim 2021; Yan et al. 2021). The ML approach is relatively new but requires a large number of site-specific observed events. The quality of observed data and ML algorithms determine the accuracy of flood prediction. However, many cities, especially in developing countries, do not have a fair amount of observed data, and this limits the application of the ML approach. In the case of the simplified hydraulic model approach, the local and convective or only convective acceleration terms are dropped out from the shallow water equations to obtain diffusive or local-inertial models (Bates et al. 2010; Kuiry et al. 2010; Prestininzi 2008; Sridharan et al. 2020). Although the simplified models improve the computation time significantly than full 2D models, they fail to produce detailed information, such as flow velocities, which are needed to prepare the flood hazard maps.

The technique of using adaptive mesh relies on a space-time-variable mesh that varies as a function of flow evolution (Berger and Colella 1989; Hu et al. 2018). The sub-grid mesh approach, on the other hand, enables the modelers to use a coarser computational grid over a high-resolution DEM. The use of a coarser grid reduces the required simulation time, while the high-resolution DEM captures the minute topographical details of urban areas, which are highly significant for capturing urban flow dynamics within a city (Chen et al. 2012; Guinot and Soares-Frazão 2006; Haltas, Elçi, et al., 2016; Haltas, Tayfur, et al., 2016; McMillan and Brasington 2007; Sanders et al. 2008). The sub-grid approach has been adopted by many researchers and is incorporated in a few available software packages such as HEC-RAS, LISFLOOD-FP, Cellular Automata (CA) based models, etc. Among these, HEC-RAS is one of the most widely used freely downloadable models owing to its superiority in capturing the spatial distribution of flow characteristics as well as the user-friendly Graphical User Interface (GUI) (Nkeki et al. 2022; Shustikova et al. 2019). Also, HEC-RAS allows the user to adapt between diffusive wave and full dynamic 2D models. Besides, the incorporation of the Geographic Information System (GIS) component (i.e., the RAS mapper) provides a convenient and efficient platform for better management, modification, and

visualization of terrain data, flow area geometry as well as simulation results. For all the above reasons, HEC-RAS has become highly popular among flood modelers.

However, a detailed study investigating the use of the sub-grid approach in HEC-RAS full 2D for modeling flooding in urbanized floodplains remains unexplored. The authors have observed that the sub-grid approach has the potential to drastically simplify the representation of typical urban features such as buildings, streets, drains, canals, etc., without resorting to different methods to consider, for example, buildings (Schubert and Sanders 2012). Though sub-grids describe urban topographical features in higher resolution, the numerical computations go on the coarse grids utilizing pre-processed relationships between stage and volume and stage and face area. Therefore, computational efficiency and accuracy are achieved simultaneously. The simulated results can be useful for real-time flood forecasting, especially for emergency action planning and hazard analysis, by avoiding time-consuming high-resolution simulation. Therefore, in this study, we make an attempt to establish the adaptability and suitability of the sub-grid-based urban flood modeling approach available within HEC-RAS through one experimental and two case studies – the experimental test case of Alpine Toce River Valley, and the Carlisle flood of 2005 in the UK, and the Chennai flood of 2015 in India. The physical model study of the Toce River Valley is studied with the flow around buildings. The experimental study is demonstrated to validate the sub-grid approach in HEC-RAS with respect to unsteady flow depths at gauges and flow dynamics around the buildings. The cities Carlisle and Chennai have urbanized floodplains with complex, varying topography and thus require high-resolution simulations even for reasonable accuracy. Through this paper, we try to establish the superior nature of the sub-grid approach in terms of accurate urban flood simulations of real-world flood events in the least computation time possible. The computation cost, the accuracy of the results obtained, and the ability to simulate real-world flood events are assessed using a comparative study between sub-grid (i.e., with fine-resolution topography) and non-sub-grid (i.e., with coarse-resolution topography) approaches. The results from this research can be of use to the modelers and disaster management authorities to decide on using the sub-grid approach for accurate and reliable urban flood modeling, inundation forecasting, and hazard zoning with regard to natural hazard analysis.

2 Two-dimensional urban flood simulation model: HEC-RAS

Hydrologic Engineering Centre - River Analysis System (HEC-RAS) was developed by the Hydrologic Engineering Centre, United States Army Corps of Engineers (USACE HEC). It is a freely downloadable software package that enables 1D and 2D simulations of steady and unsteady flows through river channels as well as over floodplains. The software has the provision to use 2D shallow water equations or 2D diffusive wave equations, depending on the simulation requirement. In particular, the selection of governing equations depends on the computational time available, the accuracy required, and the simulation scenarios, including the topographic features of the study area.

2.1 Governing equations

The governing mass and the corresponding momentum conservation equations (Eqs. 1–3) adopted in HEC-RAS (*HEC-RAS River Analysis System Hydraulic Reference Manual*, 2016) model are

$$\frac{\partial H}{\partial t} + \frac{\partial q_x}{\partial x} + \frac{\partial q_y}{\partial y} = 0 \tag{1}$$

$$\frac{\partial u}{\partial t} + u\frac{\partial u}{\partial x} + v\frac{\partial u}{\partial y} = -g\frac{\partial H}{\partial x} + \upsilon_t\left(\frac{\partial^2 u}{\partial x^2} + \frac{\partial^2 u}{\partial y^2}\right) - c_f u + f_c v \tag{2}$$

$$\frac{\partial v}{\partial t} + u\frac{\partial v}{\partial x} + v\frac{\partial v}{\partial y} = -g\frac{\partial H}{\partial y} + \upsilon_t\left(\frac{\partial^2 v}{\partial x^2} + \frac{\partial^2 v}{\partial y^2}\right) - c_f v - f_c u \tag{3}$$

where H is the water surface elevation from a datum, u and v are the components of depth-averaged velocity, and q_x and q_y are the fluxes along the x- and y-directions, t is the time, g is the acceleration due to gravity, v_t is the coefficient of horizontal eddy viscosity, c_f is the bottom friction coefficient, and f_c is the parameter accounting for Coriolis effect. In the presented simulations, the Coriolis and viscosity effects are not considered to be important.

2.2 Numerical solution

Equations (1–3) are integrated over a control volume, and the finite volume method is employed for the numerical discretization of the equations. The control volumes can be a set of non-overlapping polygons. However, arbitrary shapes of the polygons are mainly generated along the boundaries and around irregular topographical features; otherwise, square shapes mostly represent the computational domain. Each control volume is termed a cell or an element, which forms a computational grid or mesh on which numerical computation is performed. The topographical details are stored at the centroids of cells, like in a DEM, provided the grid is formed by square cells (Fig. 1a). The mass and momentum fluxes are computed through the cell faces. The flux computation depends on the selected solver. The discretized equations are then solved at each control volume for the unknowns h, q_x, and q_y at the new time level from the known time level, considering appropriate initial and boundary conditions.

The traditional numerical models adopted to solve the set of mass and momentum conservation equations use a terrain data layer and an overlying computational grid, both being of the same resolution. This approach is hereafter termed as the non-sub-grid approach henceforth, as shown in Fig. 1a. The term non-sub-grid is adopted to differentiate the traditional approach from the sub-grid one. Thus, in short, the term non-sub-grid implies that the resolution of the adopted terrain data (DEM) and the computational grid are one and the same.

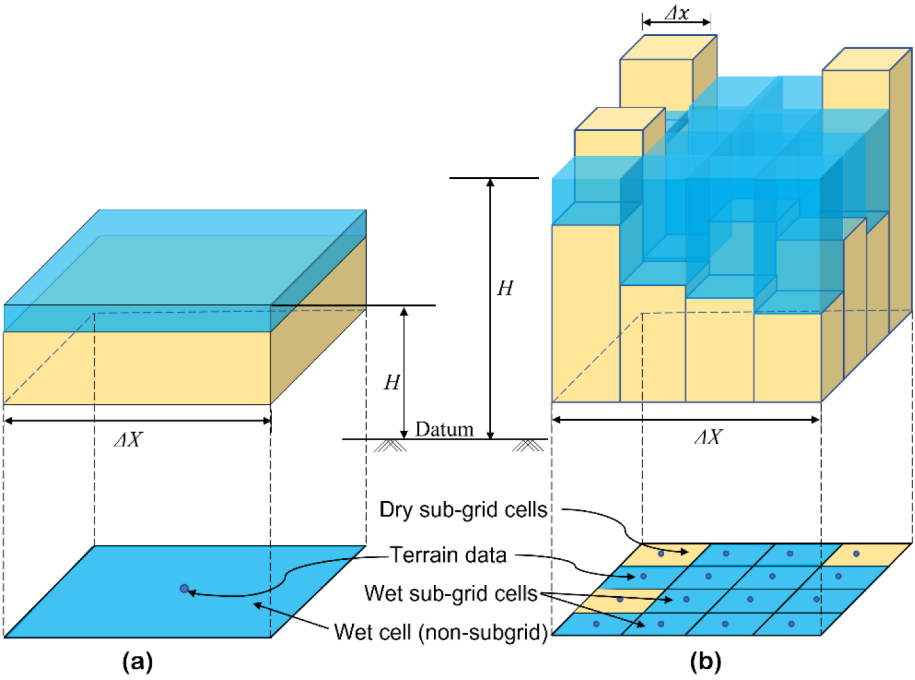

Fig. 1 Representation of the computational cell: (a) traditional non-sub-grid model and (b) sub-grid in HEC-RAS model

2.3 Concept of sub-grid for high-resolution topography

The term sub-grid denotes the use of underlying high-resolution terrain data in conjunction with an overlying coarser computational grid. Instead of coarse cells with average bed elevation (Fig. 1a) as in the case of a non-sub-grid approach, the HEC-RAS computational grids (i.e., coarse cells) have their cell features (e.g., face area, volume for flux, and flow depth computation, etc.) as a function of the high-resolution terrain described by the sub-grids (Fig. 1b) within the coarse cells (*HEC-RAS River Analysis System Hydraulic Reference Manual*, 2016). The pre-processor available within the software enables the generation of the geometric as well as hydraulic property tables at the cells and cell faces based on the input high-resolution terrain data. The hydraulic property tables compute the volume as a function of water surface elevation and conveyance through each face as a function of the face area. The face area and wetted perimeter are again defined as functions of the water surface elevation. For example, in Fig. 2, when a 30 m × 30 m computational grid is generated over a 5 m × 5 m resolution DEM, the model generates property tables such as water surface elevation vs. volume relationship depending on that high-resolution (i.e., 5 m × 5 m) DEM data available for each computational grid. The computed hydraulic tables that are prestored before the model simulation for the highlighted cell in the red box in Fig. 2 are shown in Fig. 3.

As the equations are discretized using the finite volume method, the fluxes are computed using the prestored face area, wetted perimeter, and conveyance tables, and the volume is

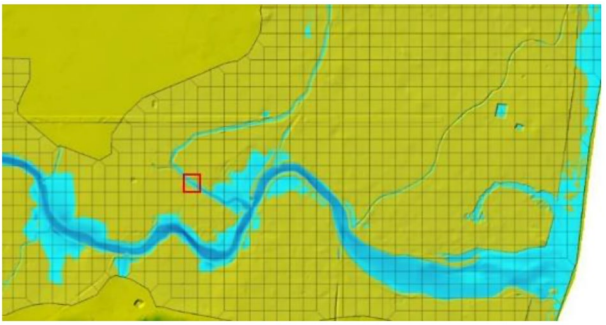

Fig. 2 Flow through narrow drains and channels as simulated by a sub-grid model in HEC-RAS

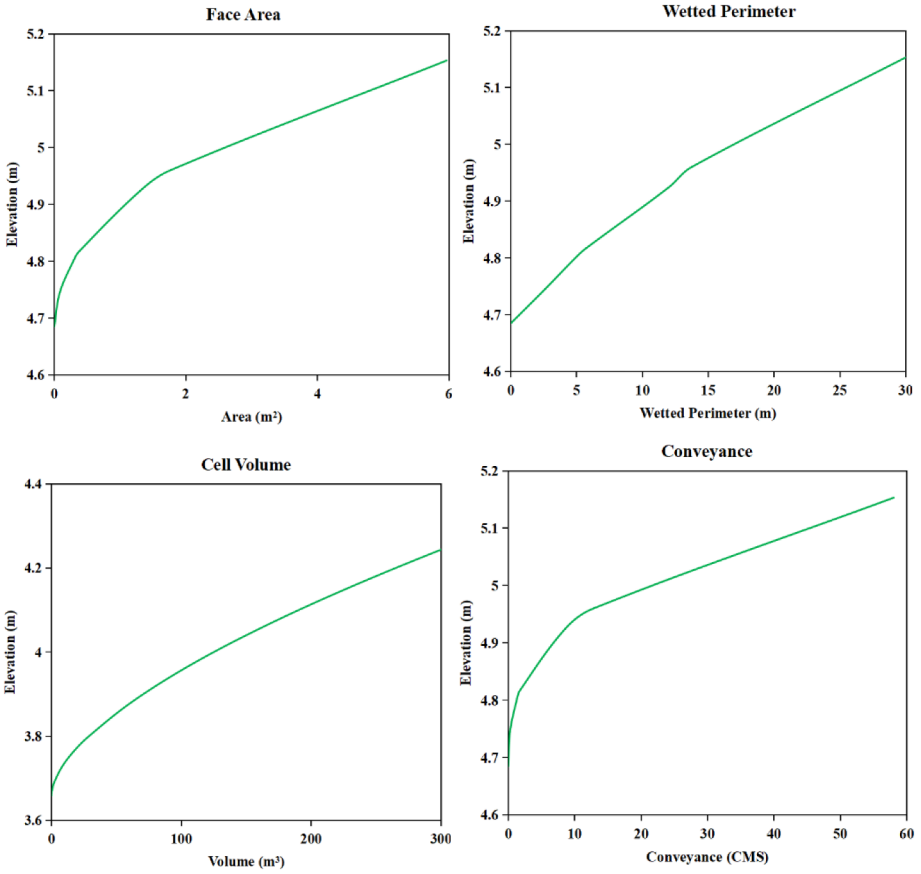

Fig. 3 Flow area property tables used in the HECRAS model for flux and water level computation

updated by adding fluxes through the coarse cell faces. Therefore, numerical computations during a simulation largely take place in the coarse cells, which are fewer in number than the sub-grid cells. The new water surface elevation for a coarse cell is then estimated based on the updated volume and the prestored volume-surface elevation table. Thus, the sub-grid

approach incorporates the high-resolution terrain data in the numerical solution of the governing equations. This improves the numerical solution, especially in an urbanized domain, and better accuracy is achieved.

2.4 Possibility of improved flow dynamics around urban features due to sub-grids

The dynamic updating of the variables based on the sub-grid geometry enables capturing the flow through narrow channels within the coarse cells, as shown in Fig. 2. Besides, high-resolution terrain beneath enables better computation of flow dynamics around and amid built-up areas by tracing the building footprint accurately. Thus, to reiterate, the significant advantage of the sub-grid approach is the representation of urban topographical features in the numerical computation without resorting to any special approach, as discussed before, for higher accuracy. This enables one to use a coarser grid with a larger time step, ensuring lower computational time but without compromising the accuracy achieved in the process (*HEC-RAS River Analysis System Hydraulic Reference Manual*, 2016). For further reference, a detailed description of the sub-grid approach is available in the latest HEC-RAS hydraulics reference manual.

It should be noted that pre-processing for establishing the relationships among volume, face area, and water surface elevation does not take much time, even for large-scale applications, as discussed later in this study. The applications presented in the upcoming sections demonstrate the advantages of the sub-grid approach over the traditional coarse-grid approach for accurate and computationally efficient urban flood simulations.

3 Urban flood simulations

The present study is carried out with the help of three cases - one experimental test case and two real-time flood events, as briefed in the subsequent sections. Urban layout, especially buildings, is incorporated in all three cases employing the building block (BB) method (Schubert and Sanders 2012). This method has been identified as the best-suited building representation technique for numerical simulations in an urban layout (Mustafa and Szydłowski 2021). This method represents the buildings by raising the base terrain below the building footprint to an acceptable height, thereby declaring them as no-flow areas. Non-sub-grid and sub-grid techniques of HEC-RAS are used to generate urban flood inundation maps for a comparative study and to find a suitable approach for urban flood simulation and risk management. For non-sub-grid computations, coarser DEMs of the resolution corresponding to the adopted computational grid are considered, while for sub-grid computations, DEMs of the higher resolution available are used as the base terrain data. Grid convergence tests are carried out for all the cases to determine the stable time step size, and only the converged solutions are reported in this paper to reduce the length of the paper.

3.1 Case study 1: toce river valley experimental test case

Flash flood experimental study on a 1:100 scaled-down laboratory model of Alpine Toce River Valley conducted by Testa et al. (Testa et al. 2007a) as part of the IMPACT project is considered here as the first case study. The model represents an urban layout of a few build-

ings (15 cm concrete cubes) in aligned and staggered patterns. Though the test case puts forth two different configurations of buildings (aligned and staggered) with low, medium, and high flow scenarios and two DEMs (original and modified), only the aligned pattern with the original DEM and low flow case is considered here to reduce the length of the paper. Figure 4 shows the model setup and the point gauge locations within the DEM. The observed water depth data at all nine gauges is available for a period of 60 s with a time step of 0.2 s for model validation.

A resampled DEM of 5 mm resolution with the building layout is used as the base terrain for the sub-grid topographical description. Computational mesh with varied grid sizes of 5, 20, 30, 40, 60, and 90 mm are adopted in the simulations. As aforementioned, the BB method adopted to represent the urban city layout rules out the requirement of varying Manning's roughness value (n) for built-up and non-built-up areas. A common value of 0.0162 $m^{-1/3}s$ (roughness value for concrete finish) is adopted henceforth, as suggested by Testa et al. (Testa et al. 2007a). The computational results corresponding to 5 mm mesh are taken as the reference solutions while comparing with the sub-grid and non-sub-grid results

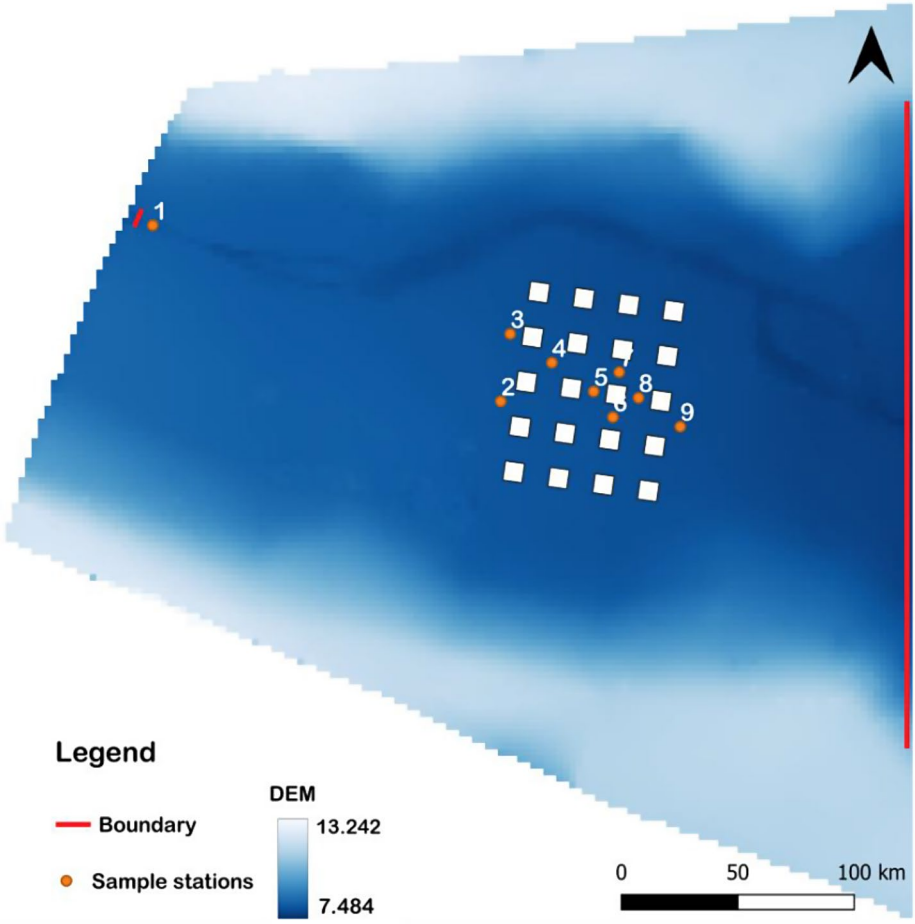

Fig. 4 Study area map – Toce experimental setup

for different mesh resolutions. Hence, the 5 mm mesh model will be referred to as the reference model – 1 (RM-1) hereafter. The inflow boundary corresponding to the inlet discharge from the upstream tank and a normal flow boundary at the downstream constitute the boundary conditions of the model as discussed by Testa et al. (Testa et al. 2007a). Simulations are carried out for a period of 60 s.

3.2 Case study 2: urban flooding of Carlisle city, UK in 2005

The city of Carlisle is the largest border city of Cumbria, lying to the north of North-West England (UK), and has three rivers - Eden, Petteril, and Caldew - flowing through the city. The city lies along 54°53′27″ N latitude and 2°56′38″ W longitude. According to the Köppen climate classification, the region has an oceanic climate with a more or less even distribution of precipitation throughout the year ("Köppen Climate Classification. Encyclopedia Britannica - Google Search," n.d.).

Carlisle has faced four major flood events since the 19th century - each in 1822, 2005, 2009, and 2015, with heavy rainfall accompanied by storms being their primary triggering factor. Among these, the urban flood that engulfed the city on January 08, 2005, succeeding a heavy downpour on the previous day, is considered the second scenario for this study. The highest recorded rainfall for this 36-hour event was 80.40 mm, with a total spell of around 175 mm (Neal et al. 2009), resembling a one in 200-year rainfall event. The peak floodwater depth was around 1 m higher than historic flood events. Figure 5 shows the study area map of the city and the sample locations for which the flow depth time-series are extracted and assessed.

A building-data incorporated DEM of 5 m resolution (Neal et al. 2009) is used as the base terrain for the sub-grid simulations of the flood event. Like in case study 1, a common Manning's n value of 0.04 $m^{-1/3}s$ is applied over the area uniformly as the building layout is well handled by the BB method. No river-bathymetry survey data is punched into the DEM due to the non-availability of the same. However, the 5 m DEM could represent the three rivers with sufficient accuracy. Computational mesh with varied grid sizes of 5, 20, 30, 40, 60, and 90 m are adopted for the study. The computational results corresponding to 5 m mesh are taken as the reference flood values and hence will be referred to as reference model – 2 (RM-2) hereafter. Three inflow boundaries corresponding to the three rivers (Eden, Caldew, and Petteril) and a normal flow boundary along the other directions constitute the boundary conditions of the model. Simulations are carried out for a period of 70 h.

3.3 Case study 3: urban flooding of Chennai city, India in 2015

Chennai, one of the densely populated coastal cities in India, lies in the North-Eastern part of Tamil Nadu, a state positioned in the South-Eastern part of India. The city holds a high degree of cultural, educational, administrative, and political significance. It falls along 13°4'2.78'' N latitude and 80°14'15.42'' E longitude. The area is predominantly flat, with three major rivers flowing through – Adyar, Coum, and Kosathalayar – and many wetlands. Though these rivers and wetlands once had abundant water and served as abodes for different aquatic species, they are presently in the face of degradation and contamination.

Chennai has a tropical wet and dry climate as per Köppen climatic classification, with fewer seasonal variations owing to its proximity to the sea and the thermal equator. North-

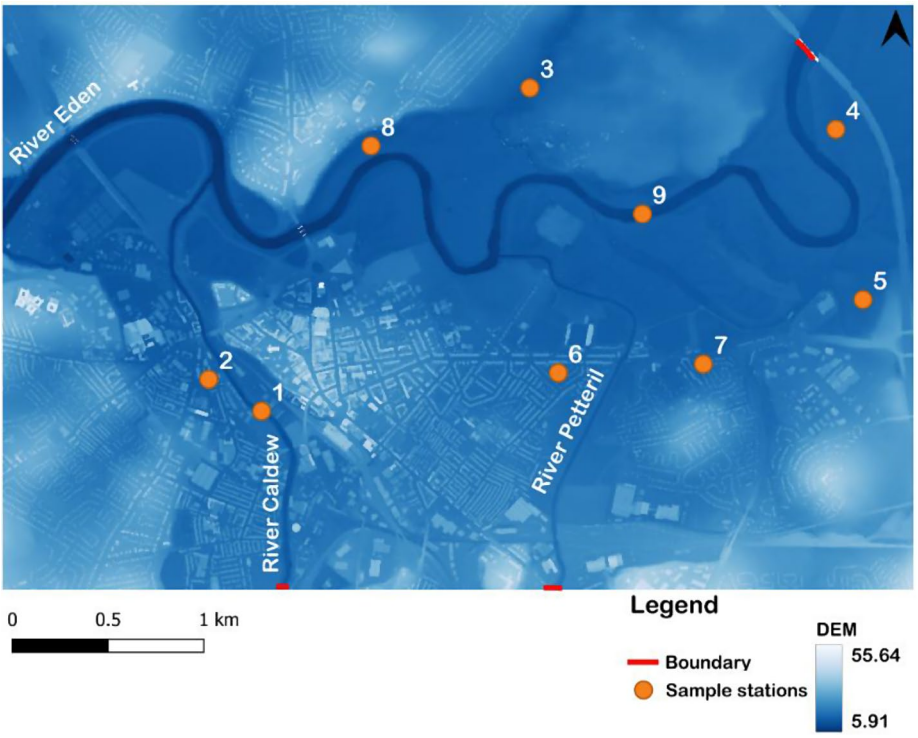

Fig. 5 Study area map – Carlisle

East monsoon during the October-December months and coastal cyclones along the Coromandel coast bring in the major amount of rainfall to the city with an average annual value of 1400 mm. Chennai has faced drastic and haphazard urbanization during the last three decades owing to industrialization and subsequent migration from rural areas. This has, in turn, shot up the probability and, hence, the frequency of flooding within the city. Floods that were once in a 10-year event have now become an annual phenomenon (Gupta and Nair 2010). Historical floods of 1943, 1978, 2005, and 2015 are the major flood events that struck the city. Among these, the 2005 and 2015 flood events caused the most destruction and losses, which may be attributed to population explosion, rapid urbanization, industrialization, and poor drainage systems.

The Chennai Metropolitan Area (CMA) lies in the downstream portion of the Adyar basin. The Adyar River flowing through the CMA overflows during heavy rainfalls and floods the adjoining city area. The flood event that struck the city on November 08, 2015, with cyclone-induced heavy rainfall inundating the area for more than a month (November 08 - December 14) is considered the third scenario for this study. The highest recorded rainfall during the event was 1049.30 mm, a one in 100-year rainfall event for the city. Figure 6 shows the study area map of Chennai city and the sample locations for which the flow depth was extracted and assessed.

A 10 m resolution resampled LiDAR DEM burnt-in with the building data is used as base terrain for the HEC-RAS sub-grid simulations. The use of high-resolution DEM (i.e.,

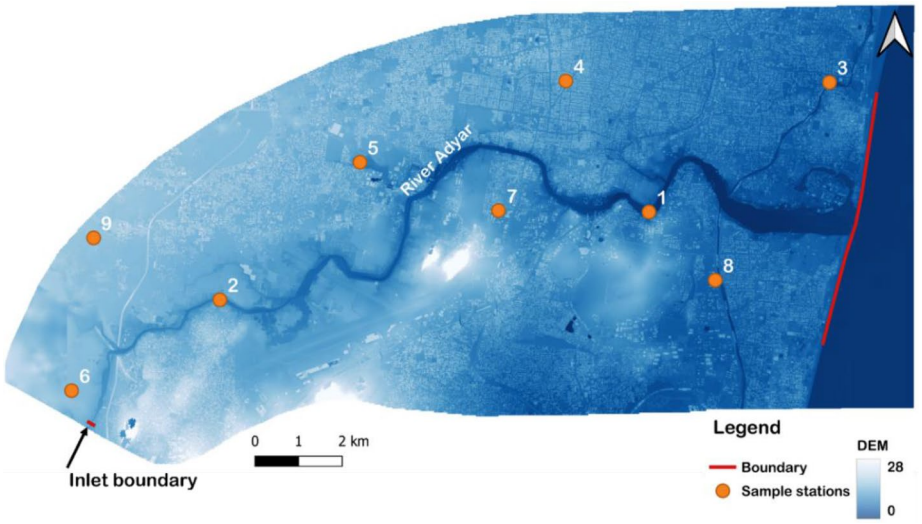

Fig. 6 Study area map – Chennai

1 m LiDAR DEM) for such a large domain is avoided due to significantly long simulation time, which could not be afforded in real-time flood forecasting, especially for emergency action planning. As in Carlisle case, no river-bathymetry survey data was punched into the DEM due to non-availability. However, a 10 m DEM is found to be apt enough to represent the Adyar River with acceptable accuracy and reliability. Computational mesh with varied grid sizes of 10, 20, 30, 40, 60, and 90 m are adopted for the study. Manning's n value of 0.035 $m^{-1/3}s$ is applied over the area uniformly, as suggested in a previous study by Nithila Devi et al. (Nithila Devi et al. 2020). For this case study, results corresponding to 10 m mesh are taken as the reference and hence will be referred to as the reference model-3 (RM-3) hereafter. Simulations are carried out for a period of 80 h. An inflow boundary across the Adyar River corresponding to the rainfall-runoff response hydrograph from the upstream basin for the 2015 flood event (Nithila Devi et al. 2019, 2020), the tidal condition at the Adyar River mouth pertaining to the same flood event (Narasimhan et al. 2016; Nithila Devi et al. 2020) where the river meets the Bay of Bengal, and normal outflow boundary along the other directions constitute the boundary conditions.

3.4 Assessment and analysis of simulation results

The time required for simulating a flood event in real-time or forecasting a flood for issuing early warnings is a crucial factor in flood risk management and damage reduction measures. However, the run time reduction factor alone is not sufficient to establish the supremacy of a modeling approach. A detailed flood flow analysis is conducted henceforth to better understand the advantages of the sub-grid approach. Time evolution of flow depth, inundation area, as well as maximum inundation extent maps, and velocity vector maps are generated for each of the runs of the three scenarios using RAS Mapper in HEC-RAS. The area of maximum inundation generated by each simulation is evaluated using the inundation maps developed with the aid of the GIS software package ArcGIS. Furthermore, flood hazard

maps and fitness indices are evaluated for each mesh size (both sub-grid and non-sub-grid) as briefed in Sect. 3.4.1 and 3.4.2, respectively. However, the hazard maps are not generated for the experimental test case as the same is irrelevant and non-applicable for an experimental model study.

3.4.1 Flood hazard map

Flood hazard maps are prepared based on the recommendations of the Department for Environment Food & Rural Affairs, the UK Government (DEFRA, 2006). The hazard index, H, is calculated as

$$H = D * (v + 0.5) + DF \tag{4}$$

where D is the flow depth, v is the velocity, and DF is the debris factor. The debris factor is taken as a non-zero parameter depending on the depth of flow, as suggested by DEFRA (Hunt 2009). Based on the most recent recommendations by DEFRA (Hunt 2009), the inundation area is classified into different hazard zones from very low hazard to danger for all (Table 1).

3.4.2 Fitness index calculation

The maximum inundation extents generated by each mesh size (sub-grid and non-sub-grid) are compared and analyzed with reference to the reference model simulation results (RM-1, RM-2, and RM-3). The overpredicted and underpredicted areas by each mesh size are assessed quantitatively with the aid of the fitness index calculated as given in Eq. (5) (Bates et al. 2006; Kuiry et al. 2010; Sridharan et al. 2021)

$$F = \frac{A}{A + B + C} * 100 \tag{5}$$

where A is the maximum inundation area predicted by the meshes as similar to the reference model, and B and C are the overpredicted and underpredicted inundation areas, respectively, by the sub-grid or non-sub-grid model in comparison to the reference model.

4 Results and discussion

The considered urban flood events and the experimental test case are simulated in HEC-RAS 6.1.0 using a 64-bit Desktop system with 11th Gen Intel(R) Core (TM) i7-1165G7 processor @ 2.80 GHz, and 32 GB RAM. The results obtained from the simulations and their analysis are elaborated in this section.

Table 1 Flood Hazard Zoning. (Source: (Surendran et al. 2008)

Hazard Index	<0.75	0.75–1.25	1.25–2.0	>2.0
Hazard to people	Very low hazard	Danger for some	Danger for most	Danger for all

4.1 Alpine toce river valley experimental test case

The experimental test case of Alpine Toce River Valley with the aligned building layout is simulated on different grid resolutions, and comparisons are made in terms of inundation area, depth, and velocity vector maps under various flood risk levels. The sub-grid resolution that converges with the reference solution is selected through various comparisons to investigate its applicability in urban flood simulation.

4.1.1 Comparison of maximum water surface elevation

The accuracy of the simulated results is quantified by comparing them with the observed data available, as reported by Testa et al. (Testa et al. 2007b) in terms of the root mean square error (RMSE), mean absolute error (MAE) and R-squared error (R^2). The performance of the RM-1 on 5 mm grids with respect to the observed maximum water surface elevations results in RMSE = 1.89 m, MAE = 1.28 m, and $R^2 = 0.63$. The error values for all the grid resolutions are summarized in Table 2. As expected, the sub-grid approach, in general, performs better than the non-sub-grid approach.

4.1.2 Comparison of time-series of water surface elevation

Time-series of water surface elevation at the nine gauges (Fig. 4) are extracted and assessed with respect to the observed values for the effectiveness of the sub-grid approach in representing the temporal evolution of the flow. Plots for four gauges are included here (Fig. 7), as the results are similar in nature and hence to reduce the length of the paper.

As seen from Fig. 7, simulations on 20 and 30 mm sub-grids yielded similar results as RM-1 and the observed data at all the stations. The results obtained for the RM-1 model are very similar to those reported from TELEMAC (Li et al. 2019) as well as dynamic-wave cellular automata (Chang et al. 2022) models. As seen in those models there is a slight over or underprediction of the observed data, which may be attributed to the difference in complex sensor measurement techniques and numerical solver mechanisms. The sub-grids beyond 30 mm as well as the non-sub-grid models result in a significant overprediction at the inlet (Fig. 7a) and an underprediction amid the buildings (Fig. 7b-d). The rate of underprediction of the water depth increases for large sub-grid models like 60 and 90 mm and the non-sub-grid models. Since the effect of under or overpredicted water depths is subsequently reflected in the inundation extent as well, the maximum inundation extents are also compared as discussed below.

Table 2 RMSE, MAE and R^2 errors on comparison of simulated and observed maximum water surface elevations

Grid size (mm)	RMSE		MAE		R^2	
	Sub-grid	Non-sub-grid	Sub-grid	Non-sub-grid	Sub-grid	Non-sub-grid
20	1.77	1.94	1.23	1.36	0.62	0.51
30	1.91	2.11	1.46	1.59	0.42	0.37
40	2.08	2.19	1.62	1.67	0.33	0.32
60	2.44	2.59	1.93	2.13	0.27	0.17
90	2.27	2.61	1.72	2.08	0.16	0.12

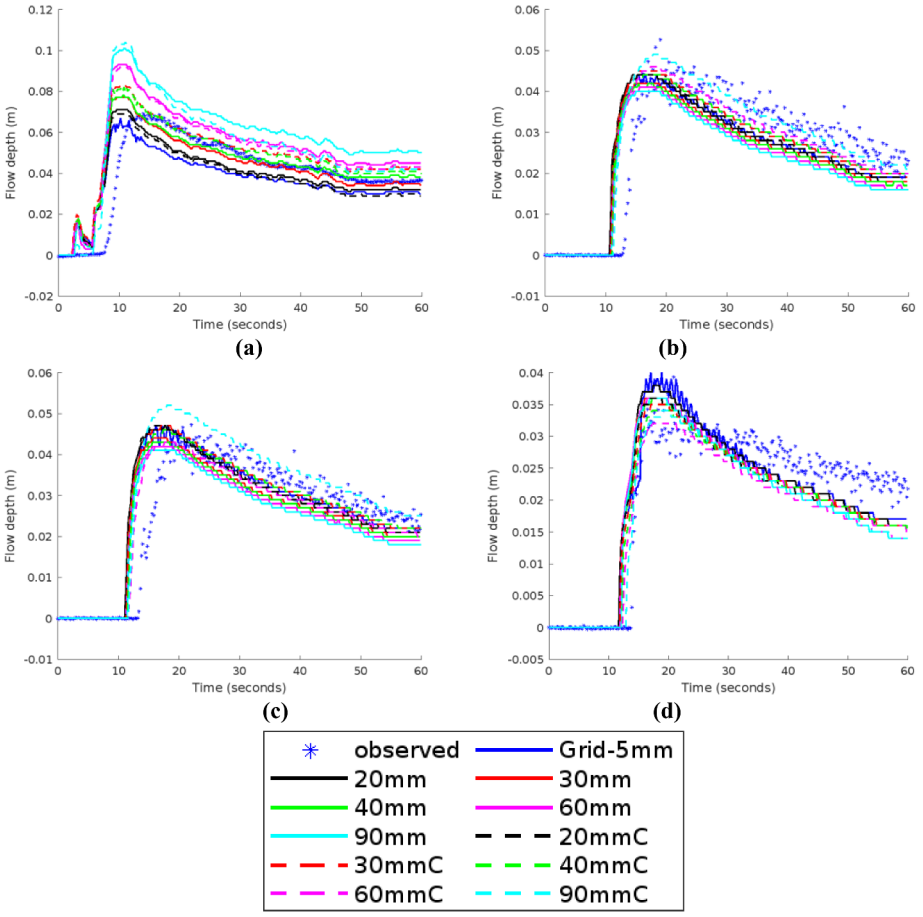

Fig. 7 Flow depth time-series for Toce flood at the gauges: (a) 1, (b) 5, (c) 8, and (d) 9. Numerals in the legend denote the adopted computational grid size, "Grid-5 mm" represents results generated by the RM-1 model with 5 mm mesh, "observed" denotes the observed value set. The solid lines with "Xmm" notation represent results from the simulation of sub-grid models using 'X' mm computational mesh, and the dashed lines with "XmmC" notation denote the results from the simulation performed with the non-sub-grid models using 'X' mm coarse computational mesh

4.1.3 Comparison of the maximum inundation extent

The observed inundation map for the test case is not available, and hence, the inundation map by RM-1 is considered to be the reference map. In order to limit the length of the paper, the maps only for 20 mm grids are shown in Figs. 8 and 9 for the sub-grid and non-sub-grid simulations, respectively. The simulated maps are overlaid on the RM-1 map so that under and overpredicted areas can be visualized. The overall inundation extent is found to be more or less the same for all the resolutions. This is because the setup is small, and building footprints do not occupy much area in the computational domain. However, the sub-grid model gives better results with reference to the RM-1 model results, for the area in the immediate vicinity of the buildings. The flow amid and around the buildings is accurately captured by

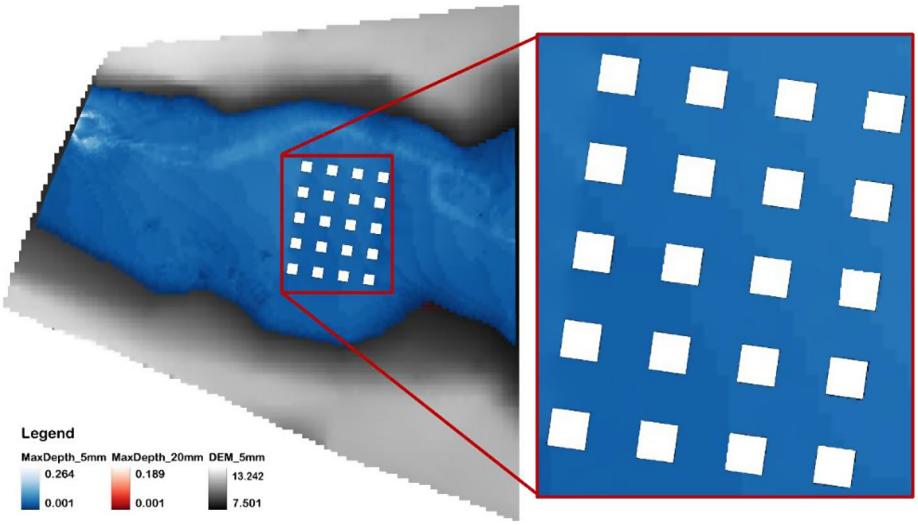

Fig. 8 Maximum inundation extent map for sub-grid simulations - Toce

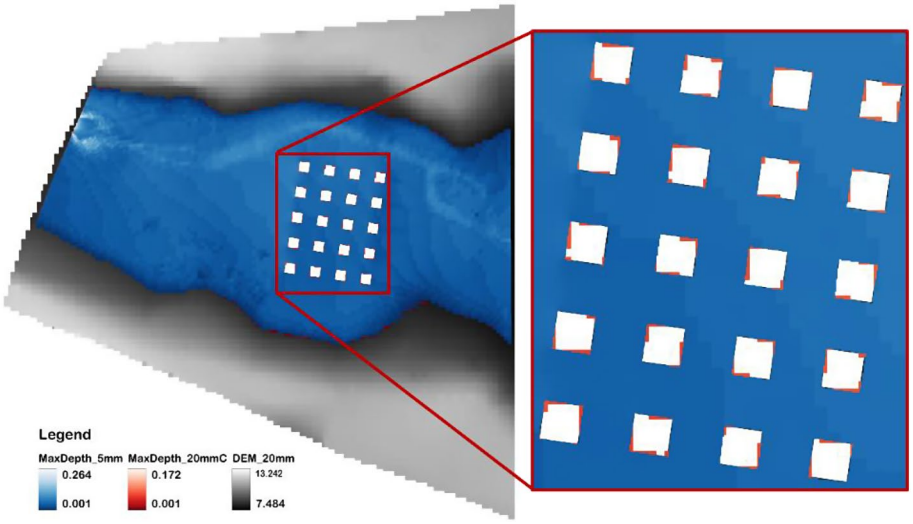

Fig. 9 Maximum inundation extent map for non-sub-grid simulations - Toce

the sub-grid model, as seen in Fig. 8 and the zoomed-in view. On the contrary, the non-sub-grid model cannot capture the inundation accurately around the urban features, as seen in Fig. 9 and the zoomed-in view. It fails to capture the exact boundary of the buildings thereby resulting in an unrealistic flow representation.

Also, there is slight overprediction along the left bottom bounding extents of inundation in the case of the non-sub-grid model. Thus, overall, the sub-grid model performs

Table 3 Fitness Index: Toce

	Sub-grid model					Non-sub-grid models				
Grid size (mm)	20	30	40	60	90	20	30	40	60	90
Fitness Index (%)	**99.2**	**98.3**	98.0	97.8	97.4	92.9	92.7	92.3	91.7	89.9

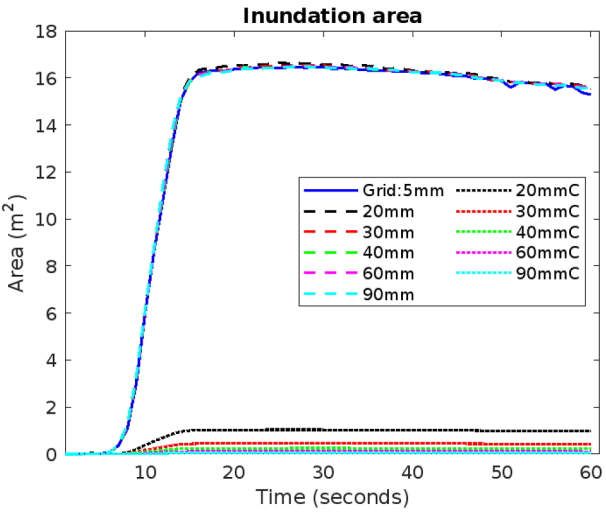

Fig. 10 Inundation area time-series graph for different grid sizes (sub-grid and non-sub-grid) –Toce River Valley experiment

better than the non-sub-grid model. The accuracy of the inundation extents for each of the grids is quantified using the fitness index given by Eq. (5) and is provided in Table 3. It can be noticed from the table that the sub-grid model predicts floods accurately compared to the non-sub-grid model. The higher fitness index value (>95%) for the sub-grid model points out its better suitability for reliable and accurate urban flood simulations. In particular, the 20 mm sub-grid has almost 100% fitness in comparison with the RM-1 model.

In addition to the maximum inundation extent, the temporal variation of the inundation area over the period of simulations is also compared, as shown in Fig. 10. It is obvious from the plot that the trend shown by RM-1 is better captured by the sub-grid models, while the non-sub-grid models render highly underpredicted values.

4.1.4 Comparison of velocity field around the buildings

The velocity field influences the flood risk and disaster management measures, including evacuation during the event, and hence the velocity vector representation available in HEC-RAS is also analyzed to emphasize the significance of the sub-grid technique in simulating flood flow within and around the built-up area. To limit the length of the paper, the velocity vectors generated by the RM-1 model, the 20 mm sub-grid model, and the corresponding 20 mm non-sub-grid model are only included here (Fig. 11). A similar trend is found for model setups of other grid sizes as well. The built-up area with aligned pattern is considered for the purpose, as shown in Fig. 11 (area enclosed by the red rectangle). As seen

from the figure, the sub-grid model generates a velocity vector pattern nearly similar to the high-resolution RM-1 model. Whereas the non-sub-grid model at 20 mm resolution fails to capture the complex flow pattern within the urban area amid the buildings and along the street. The flow field along the building footprints is accurately simulated by the sub-grid model, whereas the non-sub-grid model fails to trace the footprint. Also, the complex flow pattern amid two structures is better represented by the RM-1 and 20 mm sub-grid models (Fig. 11a-f).

4.1.5 Comparison of computation time

The net computation time required for each run for the Toce event is given in Table 4. The net computation time for the RM-1 model is 22,821 s. Thus, as seen from the table, the sub-grid model of mesh size 20 mm provides similar results as RM-1 but in a lesser simulation time. The computational time consumed by the 20 mm sub-grid model is around 0.027 times that consumed by the RM-1 model, i.e., the 20 mm sub-grid model is 36.8 times faster than the RM-1 model.

The sub-grid models with a mesh size of 20 mm produce quite accurate results with significantly less (approximately 0.027 times) computation time when compared to the full dynamic 2D model on 5 mm mesh. The coarse non-sub-grid model is faster than the sub-grid model on the same computational mesh, but the accuracy is compromised. Therefore, the sub-grid of a 20 mm computational grid can be considered the best-suited one for the simulation of experimental flood scenarios of the Alpine Toce Valley test case when using a 5 mm resolution DEM for topography description. This experimental test case validates the superiority of the sub-grid concept for simulating urban flood dynamics with respect to accuracy and simulation time.

4.2 Carlisle flood of 2005

The Carlisle flood event is simulated on different grid resolutions, and comparisons are made in terms of inundation area, depth, velocity field, and hazard maps under various flood risk levels, as in the Toce Valley event.

4.2.1 Comparison of maximum water surface elevation

The accuracy of the simulated results is quantified by comparing the simulated maximum water surface elevations with the observed data available for the area, as reported and used by Neal et al. (Neal et al. 2009) and Liu and Pender (Liu and Pender 2013) in terms of the root mean square error (RMSE), mean absolute error (MAE) and R-squared error (R^2). The performance of the RM-2 on 5 m grids with respect to the observed maximum water surface elevations results in RMSE = 0.77 m, MAE = 0.72 m, and $R^2 = 0.82$. The error values for all the grid resolutions are summarized in Table 5. As expected, the sub-grid approach, in general, performs better than the non-sub-grid approach. The value of the R^2 error is found to reduce with an increase in the mesh size beyond 30 m. For all the non-sub-grid resolutions, the R^2 value is less than 0.4, again indicating the better performance of the sub-grid model. The RMSE and MAE values of 20 and 30 m sub-grid setups are comparable with the HEC-RAS reference results.

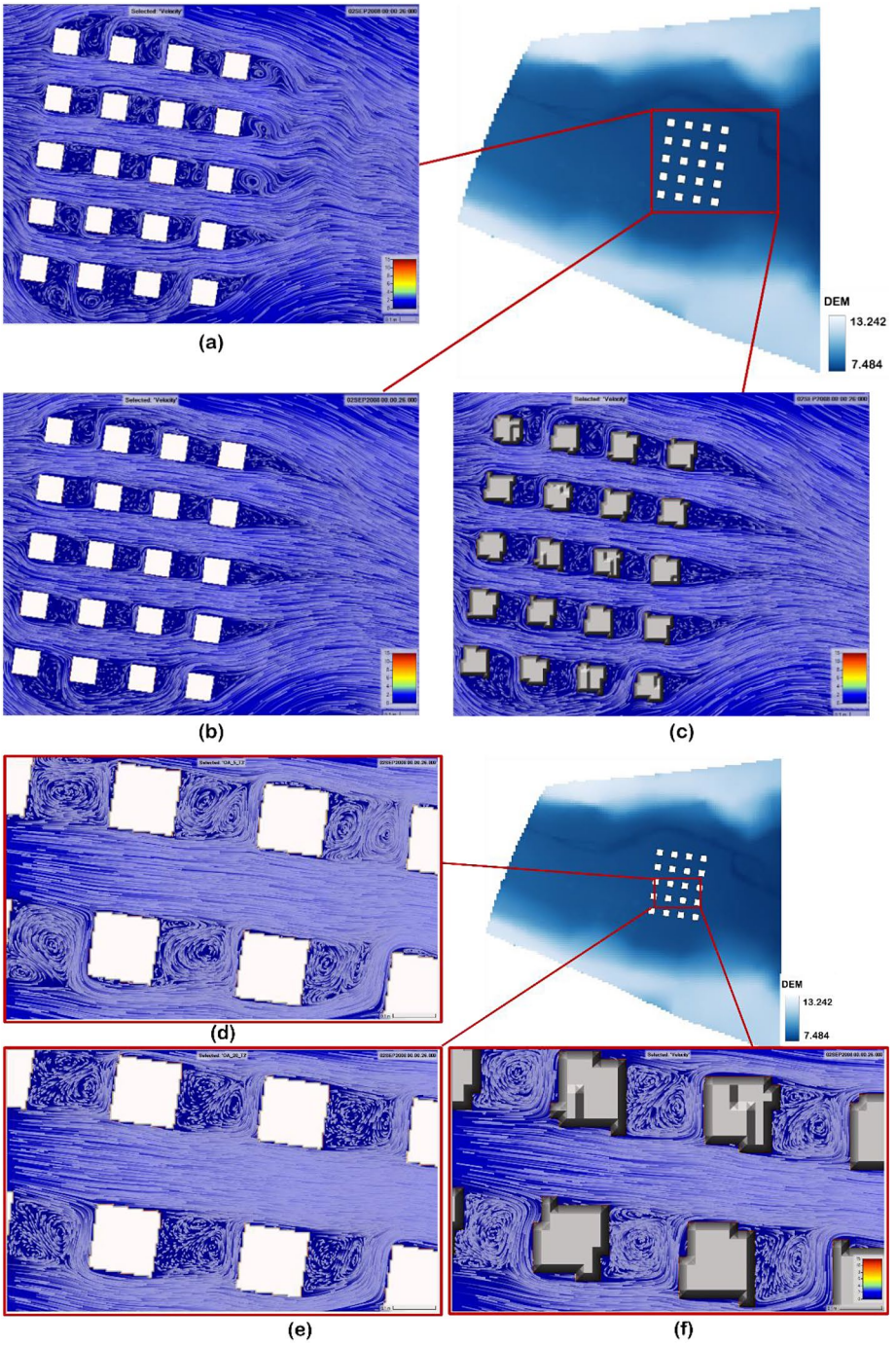

Fig. 11 Velocity Vector Representation – Toce for: (a) RM-1, (b) 20 mm sub-grid model, (c) 20 mm non-sub-grid models, zoomed in views for (d) RM-1, (e) 20 mm sub-grid model, (f) 20 mm non-sub-grid model

Table 4 Total computation time for each grid size

Grid size (mm)	Total run time (hh:mm:ss)		Total run time (s)		Relative run time with respect to RM-1	
	Sub-grid	Non-sub-grid	Sub-grid	Non-sub-grid	Sub-grid	Non-sub-grid
20	00:10:20	00:10:06	620	606	0.027	0.026
30	00:04:12	00:04:00	252	240	0.011	0.010
40	00:02:23	00:02:20	143	140	0.006	0.006
60	00:01:00	00:01:00	60	60	0.002	0.003
90	00:00:18	00:00:18	18	18	0.001	0.0007

Table 5 RMSE, MAE and R^2 errors on comparison of simulated and observed maximum water surface elevations

Grid size (m)	RMSE		MAE		R^2	
	Sub-grid	Non-sub-grid	Sub-grid	Non-sub-grid	Sub-grid	Non-sub-grid
20	0.718	0.979	0.656	0.662	0.815	0.380
30	0.769	1.239	0.717	0.782	0.821	0.284
40	0.886	1.742	0.819	1.042	0.796	0.105
60	1.099	1.823	1.035	1.105	0.764	0.078
90	1.262	2.047	1.194	1.256	0.742	0.046

4.2.2 Comparison of time-series of water surface elevation

A few locations are selected hypothetically across the study area comprising the main river Eden and its tributaries Caldew and Petteril and the surrounding urban area, as shown in Fig. 5. The water depths are reported at these hypothetical locations to demonstrate the effectiveness of the sub-grid approach in representing the evolution of the urban flood with time. The time-series of flow depths obtained using the RM-2 are used to compare the sub-grid and non-sub-grid model results at the selected locations, owing to the lack of observed time-series data of water depths, as shown in Fig. 12.

All the sub-grid models provide similar flow trends in the river and over the barren land as that of RM-2, while the significance of the sub-grid approach is highly prominent in the representation of flow in urban areas. It can be observed from Fig. 12 that the 20 and 30 m sub-grids yielded similar results as RM-2 at all the stations. The non-sub-grid models result in a significant underprediction of flow depths in the rivers (12 a and h) and an overprediction in the barren lands (Fig. 12d and g). Also, the non-sub-grid models fail to represent the flow trend, particularly amid the buildings (Fig. 12b and f). The rate of underprediction of the water depth increases for large sub-grid models like 60 and 90 m and the non-sub-grid models.

The non-sub-grid models generally fail to capture the underlying terrain features due to the coarser DEM used, and hence, the flow arrival is not accurately captured. In this case, this results in overflowing the river onto floodplains (barren land) before reaching the actual peak, thus underpredicting the river flow depth and consequently causing early flooding of floodplains, as seen in Fig. 12d and g. Also, since the flow from the floodplains to the river is not captured properly, the peak in barren land is higher than the reference solution. From a grid sensitivity point of view, we can say that the results tend to diverge with the coarsening (from 30 to 90 m) of cell size, especially in the case of non-sub-grid model. As seen from

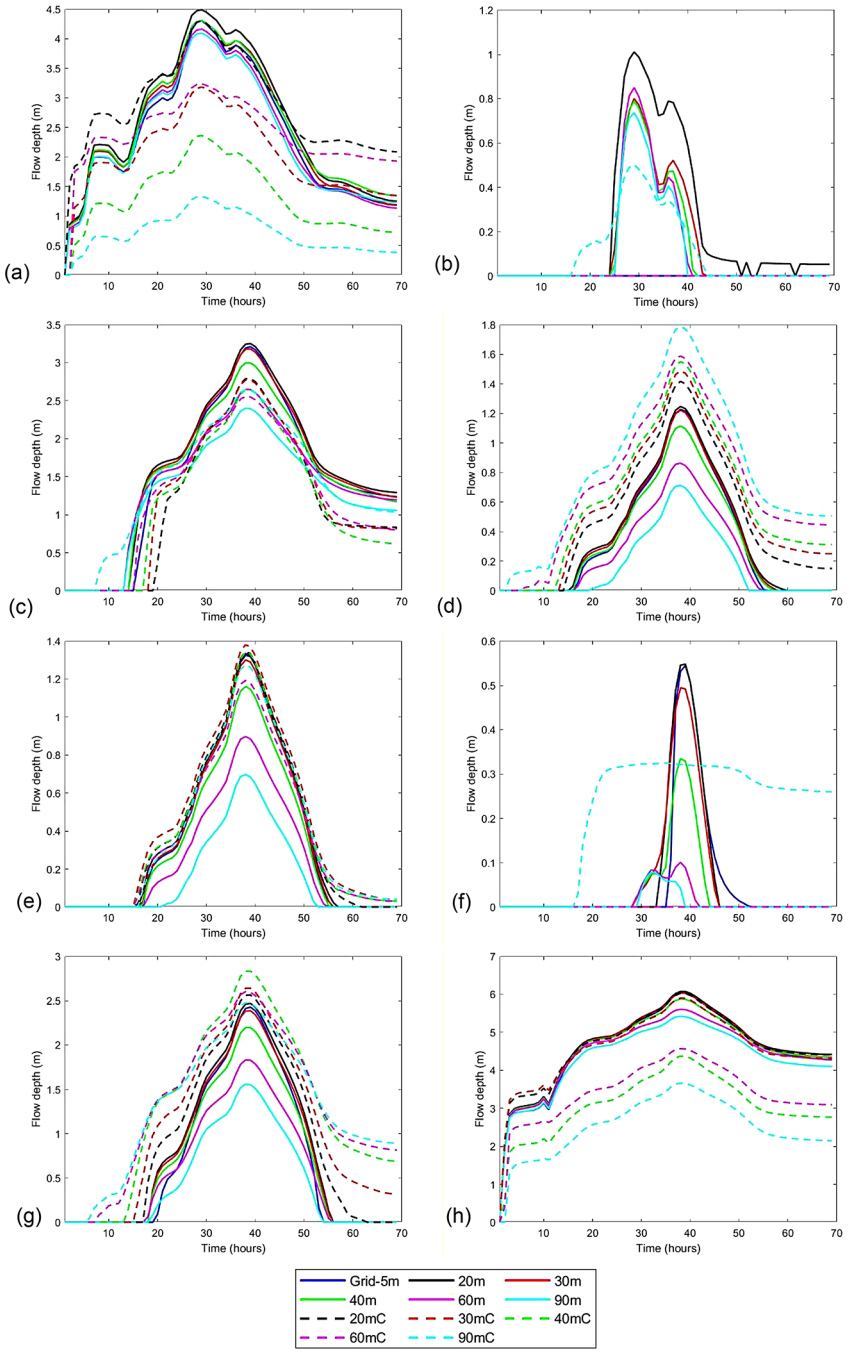

Fig. 12 Flow depth time-series at selected locations - Carlisle flood: (a) Caldew River, (b) and (f) Urban area, (c), (d), (e), and (g) Barren land, (h) Eden River. Numerals in the legend denote the adopted computational grid size, and the capital letter 'C' represents the coarser grid or non-sub-grid models. For example, 'Xm' solid lines denote the results from the simulation using sub-grid models with X m computational mesh, and 'XmC' dashed lines denote the results from the simulation performed using non-sub-grid models with X m coarser mesh

Fig. 12d and g, when we coarsen the sub-grid, though the flow characteristics, trend, and flooding-residing pattern are still well captured, the accuracy tends to reduce. In summary, a non-subgrid model needs to be checked for grid sensitivity as usual. On the other hand, site-specific trials need to be carried out to find out the optimal combination of the sub-grid resolution for terrain and numerical grid resolution for flux computation for acceptable accuracy and computation time. The effect of under or overpredicted water depths is subsequently reflected in the inundation extent as well as discussed below.

4.2.3 Comparison of the maximum inundation extent

The observed satellite inundation map for this event is not available, and hence, the inundation map by RM-2 is considered to be the reference map. In order to limit the length of the paper, the maps only on 30 m grids are shown in Figs. 13 and 14 for the sub-grid and non-sub-grid simulations, respectively, as in case study 1. The simulated maps are overlaid on the RM-2 map so that under and overpredicted areas can be visualized. The inundation map over the barren floodplains and the river system is found to be more or less the same for all the models. However, the sub-grid model gives better results with reference to the RM-2 model results. The street flooding and flow amid buildings are accurately captured by the sub-grid model, as seen in Fig. 13 and the zoomed-in view. On the contrary, the non-sub-grid model cannot capture the inundation accurately around the urban features, as seen in Fig. 14 and the zoomed-in view. It mostly overpredicts the flow and inundation amid the buildings.

The overprediction along these rivers by the sub-grid model may be due to the approximation that arises due to the flux computation by the interpolated relationships as adopted by the HEC-RAS sub-grid formulation. However, the non-sub-grid model results in overprediction due to an inaccurate description of the river and floodplain topography. Although both the model setups show overprediction along the floodplains of the rivers Caldew and Petteril and in some other regions, overall, the sub-grid model performs comparatively better than the non-sub-grid model. The accuracy of the inundation extents for each of the grids is quantified using the fitness index given by Eq. (5) and is provided in Table 6. It can be noticed from the table that sub-grid models of 20 and 30 m grids predict floods accurately compared to other sub-grid and non-sub-grid models. The higher fitness index value (>95%) for 20 and 30 m sub-grid models points out their better suitability for reliable and accurate urban flood simulations. In contrast, the non-sub-grid model setups show 9.9% and 13.4% lesser accuracy than the corresponding sub-grid model setups for 20 and 30 m grid sizes, respectively.

In addition to the maximum inundation extent, the hourly variation of inundation area over the period of simulations is also compared, as shown in Fig. 15. It is obvious from the plot that the trend shown by RM-2 is better captured by 20 and 30 m sub-grid models, while the 90 m sub-grid model and the non-sub-grid models render an entirely different pattern. The flooding and receding phenomenon are also well captured by the sub-grid model. All the non-sub-grid models, in general, overpredict the inundation area, especially during the rising and receding intervals of the flooding event.

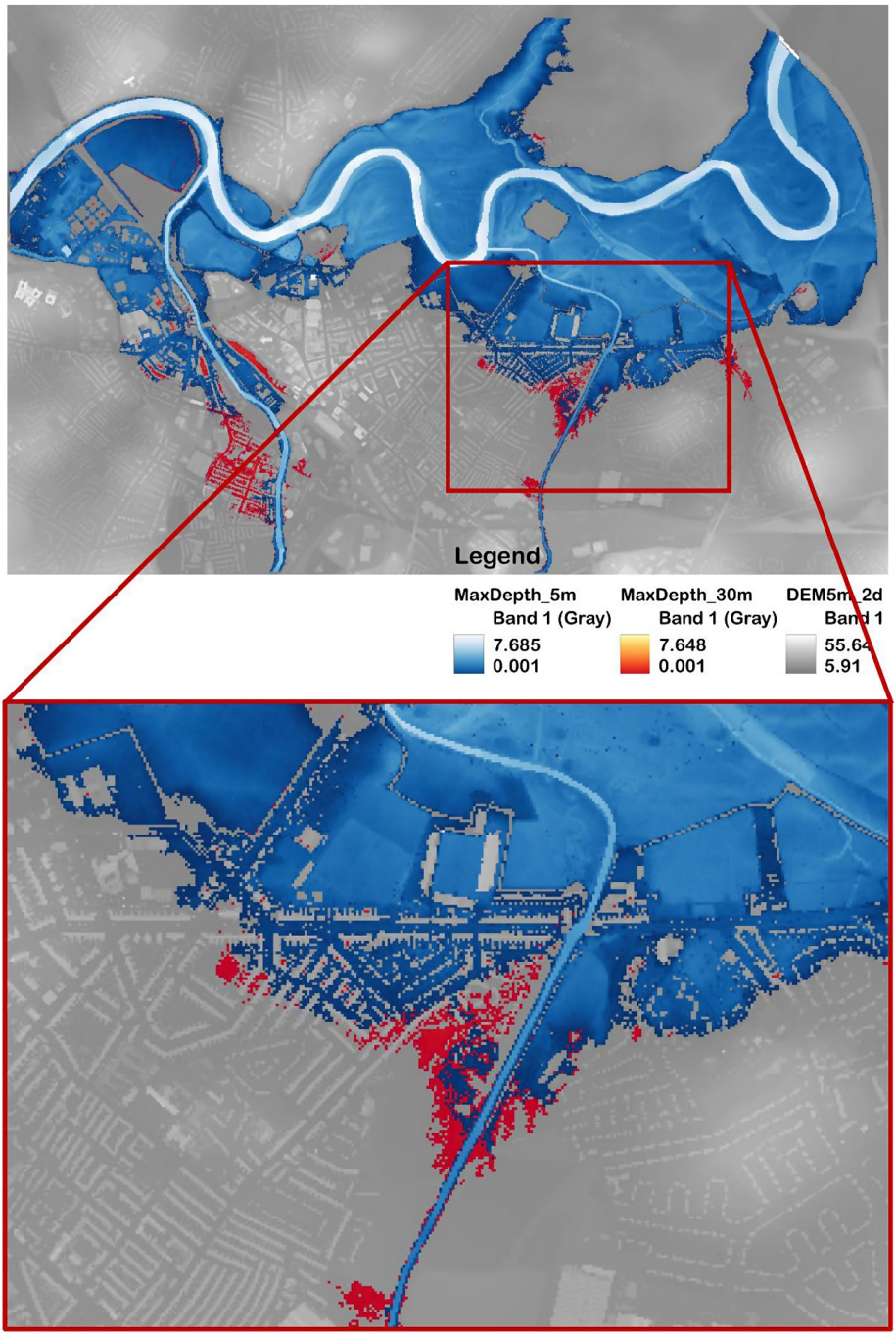

Fig. 13 Maximum inundation extent map for sub-grid simulations - Carlisle

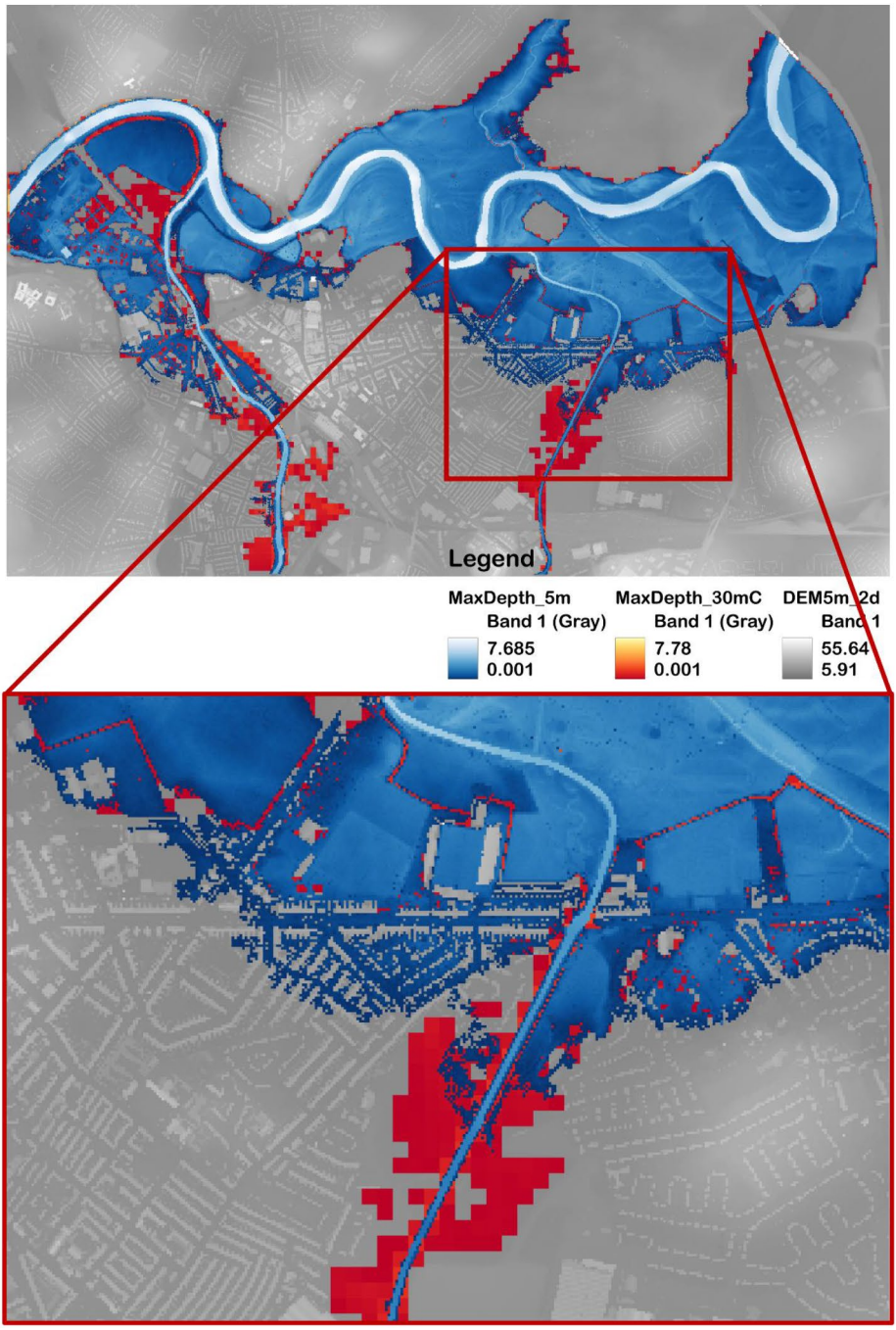

Fig. 14 Maximum inundation extent map for non-sub-grid simulations - Carlisle

Table 6 Fitness Index: Carlisle flood 2005

	Sub-grid models					Non-sub-grid models				
Grid size (m)	20	30	40	60	90	20	30	40	60	90
Fitness Index (%)	**96.4**	**96.3**	91.9	86.4	83.0	86.5	82.9	81.1	77.4	76.8

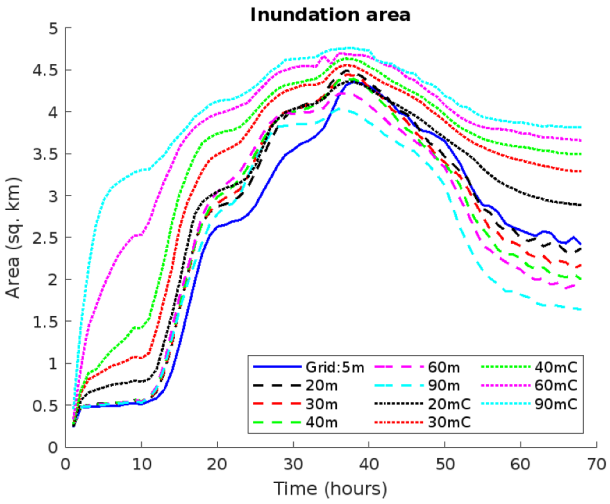

Fig. 15 Inundation area time-series graph for different grid sizes (sub-grid and non-sub-grid) – Carlisle

4.2.4 Comparison of velocity field around the buildings

The estimation of the velocity field for various model setups is summarized here. The velocity vectors generated by the RM-2 model, the 30 m sub-grid model, and the corresponding 30 m non-sub-grid model are only included here (Fig. 16) to limit the length of the paper, as in the case of Toce Valley simulations. A similar trend is found for model setups of other grid sizes as well. The urban area near Petteril River is considered for the purpose, as shown in Fig. 16 (area enclosed by the red rectangle). As seen from the figure, the sub-grid model generates a velocity vector pattern nearly similar to the high-resolution 5 m RM-2 model. Whereas the non-sub-grid model fails to capture the complex flow within the urban area amid the buildings and along the street. The real-time flow field within the urban settlement is accurately simulated by the sub-grid model, whereas the non-sub-grid model fails to generate the complex urban flow field and hence generates a flow over the buildings irrespective of the relative water depth or building height.

4.2.5 Comparison of flood risk and hazard maps

Flood risk maps and areas under each hazard zone, as generated by the simulations of each mesh size, are prepared. The hazard maps for 20 and 30 m, along with the RM-2, are only presented in Fig. 17 (a - e) in order to restrict the length of the paper. However, Table 7 summarizes hazard areas under each category and for all the considered grid resolutions. Green represents very low hazard zones, yellow represents a danger for some, orange denotes danger for most, and red represents a danger for all. The results obtained using 20 and 30 m sub-grid models are found to have a high agreement with the results of RM-2. In particular,

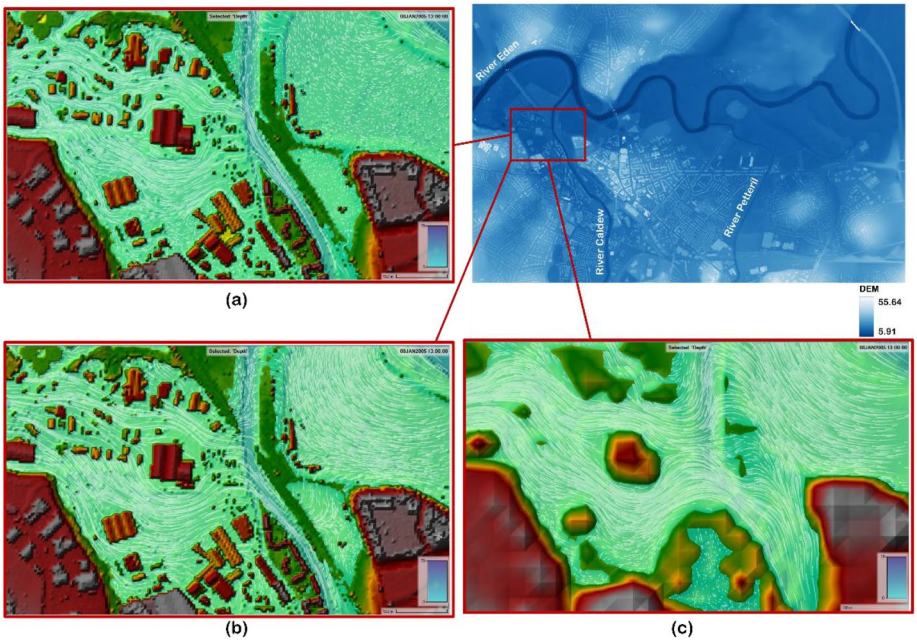

Fig. 16 Velocity Vector Representation – Carlisle for: (a) RM-2, (b) 30 m sub-grid model, and (c) 30 m non-sub-grid model

for the 20 m sub-grid and non-sub-grid model setups, the area simulated under the 'Danger for most' category is underpredicted by around 3.4% and 20%, respectively. This signifies the use of the sub-grid approach for accurate flood risk mapping. Also, a further increase in mesh size is found to cause either overprediction or underprediction of the inundation extent and, hence, the hazard zone areas. Besides, the results produced by 20 and 30 m sub-grid models are almost the same, while the coarsest mesh used (90 m - both sub-grid and non-sub-grid model) underpredicts the highly hazardous zone the most.

4.2.6 Comparison of computation time

The net computation time required for each run for the Carlisle event is given in Table 8. The net computation time for the RM-2 model is 13,412 s. Thus, as seen from the table, sub-grid models of mesh size 20 and 30 m provide the same results as RM-2 but in a shorter time span for the Carlisle flood event as well. The computational time consumed by the 20 and 30 m sub-grid mesh is, respectively, around 0.104 and 0.012 times that consumed by the RM-2 model, i.e., the 20 and 30 m sub-grid models are 8.3 and 73.6 times faster than the RM-2 model.

Thus, the 30 m sub-grid model generates quite accurate results with significantly lesser (approximately 0.012 times) computation time and hence the sub-grid of a 30 m computational grid can be considered the best-suited one for the simulation of real-time urban flood scenarios of Carlisle city when using a 5 m resolution DEM.

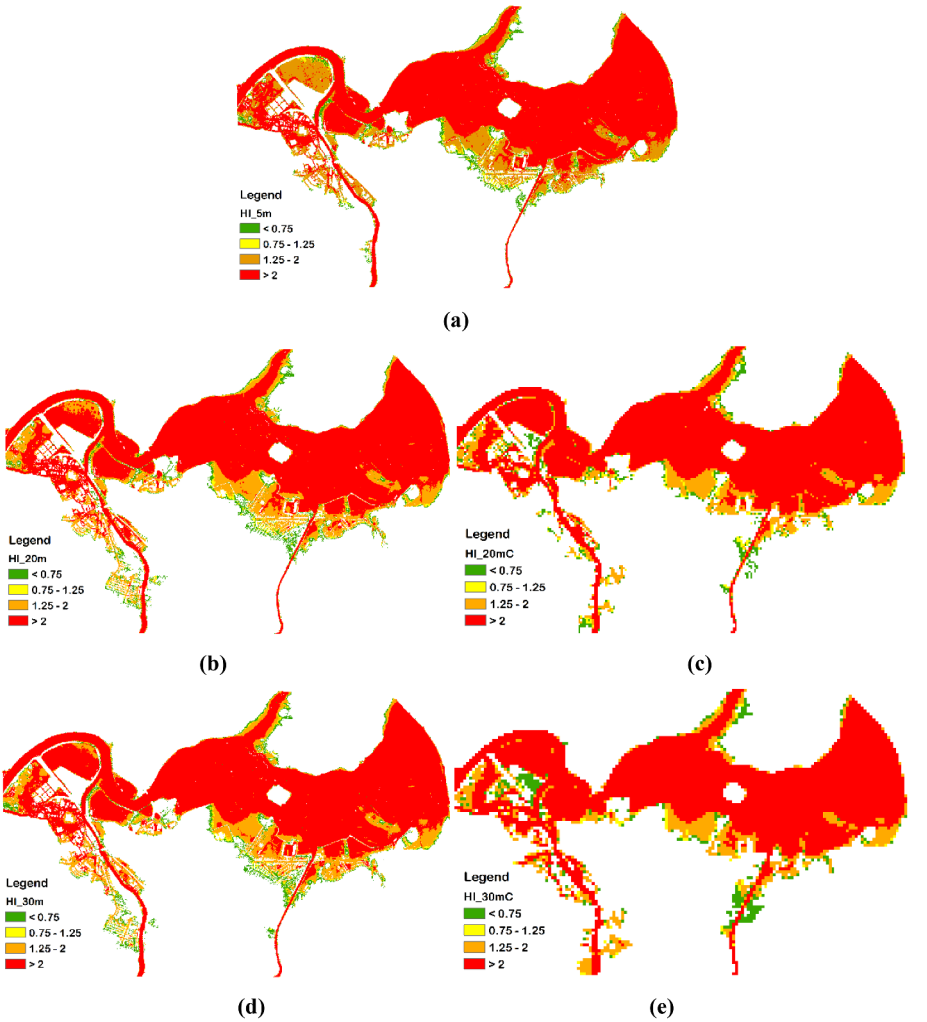

Fig. 17 Hazard Maps – Carlisle for: (a) RM-2, (b) 20 m sub-grid model, (c) 20 m non-sub-grid model, (d) 30 m sub-grid model, and (e) 30 m non-sub-grid model

Table 7 Area under each hazard zone for Carlisle city

Grid size (m)	Area under each hazard zone (sq. km)							
	Very low hazard		Danger for some		Danger for most		Danger for all	
	Sub-grid	Non-sub-grid	Sub-grid	Non-sub-grid	Sub-grid	Non-sub-grid	Sub-grid	Non-sub-grid
5	0.2		0.12		0.84		3.26	
20	0.25	0.23	0.11	0.10	0.81	0.67	3.42	3.43
30	0.25	0.25	0.10	0.09	0.76	0.75	3.42	3.54
40	0.31	0.25	0.13	0.09	0.74	0.76	3.33	3.59
60	0.27	0.27	0.10	0.11	0.84	0.80	3.13	3.60
90	0.27	0.16	0.08	0.10	0.96	0.83	2.85	3.74

Table 8 Total computation time for each grid size

Grid size (m)	Total run time (hh:mm:ss)		Total run time (s)		Relative run time with respect to RM-1	
	Sub-grid	Non-sub-grid	Sub-grid	Non-sub-grid	Sub-grid	Non-sub-grid
20	00:23:17	00:21:54	1397	1314	0.1042	0.0979
30	00:02:37	00:01:48	157	108	0.0117	0.0081
40	00:01:44	00:01:27	104	87	0.0078	0.0065
60	00:00:40	00:00:38	40	38	0.0029	0.0028
90	00:00:19	00:00:16	19	16	0.0014	0.0011

Table 9 RMSE, MAE, and R^2 errors on comparison of simulated and observed maximum water surface elevations – Chennai 2015 flood

Grid size (m)	RMSE		MAE		R^2	
	Sub-grid	Non-sub-grid	Sub-grid	Non-sub-grid	Sub-grid	Non-sub-grid
20	0.802	1.073	0.601	0.824	0.850	0.778
30	0.809	1.076	0.606	0.873	0.842	0.775
40	0.876	1.488	0.690	1.234	0.841	0.647
60	0.879	1.501	0.704	1.323	0.838	0.555
90	0.947	1.566	0.772	1.340	0.830	0.487

4.3 Chennai flood of 2015

Similar to case studies 1 and 2, the Chennai flood simulations on different grid sizes are analyzed here to identify the suitable grid size for the sub-grid model.

4.3.1 Comparison of maximum water surface elevation

As aforementioned, the accuracy of the simulated results is quantified by comparing them with the observed data available for the area, as shown in Table 9. The performance of the RM-3 on 10 m grids with respect to the observed maximum water surface elevations results in RMSE = 0.832 m, MAE = 0.635 m, and $R^2 = 0.848$. Results similar to that of the Toce and Carlisle cases are obtained, with the RMSE and MAE values being the least for 20 and 30 m sub-grid models. Also, the R^2 value is found to reduce significantly beyond a mesh size of 30 m. As seen earlier, RMSE and MAE values of 20 and 30 m sub-grid models are comparable with HEC-RAS reference results.

4.3.2 Comparison of time-series of water surface elevation

As for case study 2, flow depth time-series plots are prepared at selected arbitrary locations (Fig. 6). The locations are selected uniformly across the area of study and cover the Adyar River course within the city. The time-series of depth at the selected locations are extracted and plotted for all the adopted mesh sizes (sub-grid and non-sub-grid), as shown in Fig. 18. A trend similar to that seen in Carlisle event simulations is found for the different mesh sizes of sub-grid and non-sub-grid models. Sub-grid model with grid sizes 20 and 30 m produces results similar to RM-3, while those with 60 and 90 m mesh sizes and the non-sub-grid model either underpredicts or overpredicts the inundation depth. This reinforces the fact

that merely increasing mesh size to achieve less computation time will not render accurate results. Besides, the flow amid the buildings and streets (sample stations no. 3, 4, 7, and 9) is better captured by the sub-grid meshes when compared to the non-sub-grid ones. A close analysis of the time-series of flow depth within the riverbank confinements (Fig. 18a and b) reinforces the reduction in computation time without compromising the accuracy when the sub-grid approach is adopted. The legend notations are same as explained earlier in Sect. 4.2.2.

4.3.3 Comparison of maximum inundation extent

The maximum inundation extent maps generated by the sub-grid and non-sub-grid simulations (and the zoomed-in views) are shown in Figs. 19 and 20, respectively. Flood inundation extent over the barren floodplains and the river is more or less the same for all the models. In particular, the 30 m sub-grid model produces results in high agreement with

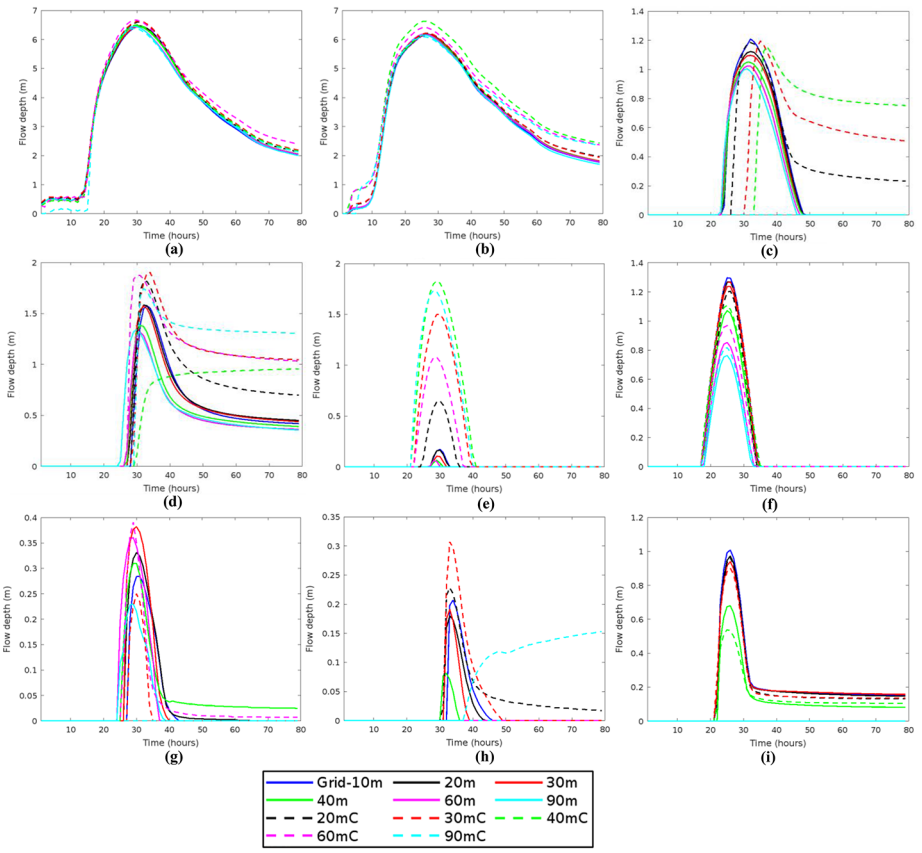

Fig. 18 Flow depth time-series at selected locations – Chennai flood: (a) and (b) – Adyar River, (c), (g), (h), and (i) – urban area, (d) and (e) street, and (f) barren land. Numerals in the legend denote the adopted computational grid size, and the capital letter 'C' represents the coarser grid or non-sub-grid models. For example, 'Xm' solid lines denote the results from the simulation using sub-grid models with X m computational mesh, and 'XmC' dashed lines denote the results from the simulation performed using non-sub-grid models with X m coarser mesh

RM-3 in terms of flood inundation extent and flow depth. Also, the flood flow pattern within the city area and amid the buildings (stations 3, 7, and 9) as well as streets (stations 4 and 5) is better captured by the smaller grid sizes, 20 m, and 30 m, with the sub-grid approach (refer Fig. 18: (c), (d), (e), (g), (h), and (i)). The red-colored regions represent the overpredicted areas generated by sub-grid and non-sub-grid models with reference to RM-3 for the same reasons as described before. Also, visually it can be seen that the coarser non-sub-grid model for the same 30 m grid generated a greater percentage of overpredicted inundation area throughout the domain (Fig. 20 and the zoomed-in view).

The fitness value of the simulation models is quantified using Eq. (5) and is provided in Table 10. It can be noticed that the sub-grid models with 20 and 30 m computational grids outperform compared to other sub-grid and non-sub-grid models considered. The higher fitness index value (>95%) for 20 and 30 m models once again shows their better suitability for reliable and accurate urban flood simulations. The non-sub-grid models for 20 and 30 m grid resolutions reported 10.7% and 13.6% lesser fitness accuracy, respectively, than the sub-grid model setups of similar grid sizes.

The hourly variation of inundation area over the period of simulations is extracted and plotted as shown in Fig. 21. It is evident from the graph that the trend shown by RM-3 is better captured by the 20 and 30 m sub-grid mesh, while the 90 m sub-grid one and other coarser non-sub-grid models render an overpredicted inundation extent, especially when the flood is receding. Nevertheless, the 20 m sub-grid model slightly overpredicts the flood peak, whereas the 30 m sub-grid mesh generates almost similar results as RM-3 except for the last segment of the recession limb.

4.3.4 Comparison of velocity field around the buildings

The velocity vector representation is analyzed, as earlier, to emphasize the superiority of the sub-grid technique. As aforementioned, to limit the length of the paper, the velocity vector generated by the RM-3 model, 30 m sub-grid model, and 30 m non-sub-grid model are only included here. The urban area near Raja Annamalai Puram (R. A. Puram) is considered for the purpose, as shown in Fig. 22 (area bounded by the red rectangle). As seen from the figure, the flow field amid the urban land is better captured by the 30 m sub-grid model than the non-sub-grid one in comparison with the RM-3 model. A similar trend is found for other models as well, similar to case studies 1 and 2. Thus, the complex flow vectors found within an urban area are best simulated by the sub-grid models, enabling them to be the apt model for urban flood simulations.

4.3.5 Comparison of flood risk and hazard maps

Flood hazard maps and corresponding areas under each hazard zone as generated by the simulations of each mesh size are prepared and are shown in Fig. 23 (a – e) and Table 11, the color representation being the same as that in the Carlisle case study, as explained in Sect. 4.2.5. The results obtained using 20 and 30 m sub-grid models are found to be in high agreement with the results of RM-3. Also, a further increase in the mesh is found to cause either overprediction of safer regions or underprediction of high-hazard zones. All the non-sub-grid models result in underprediction of high-hazard zones.

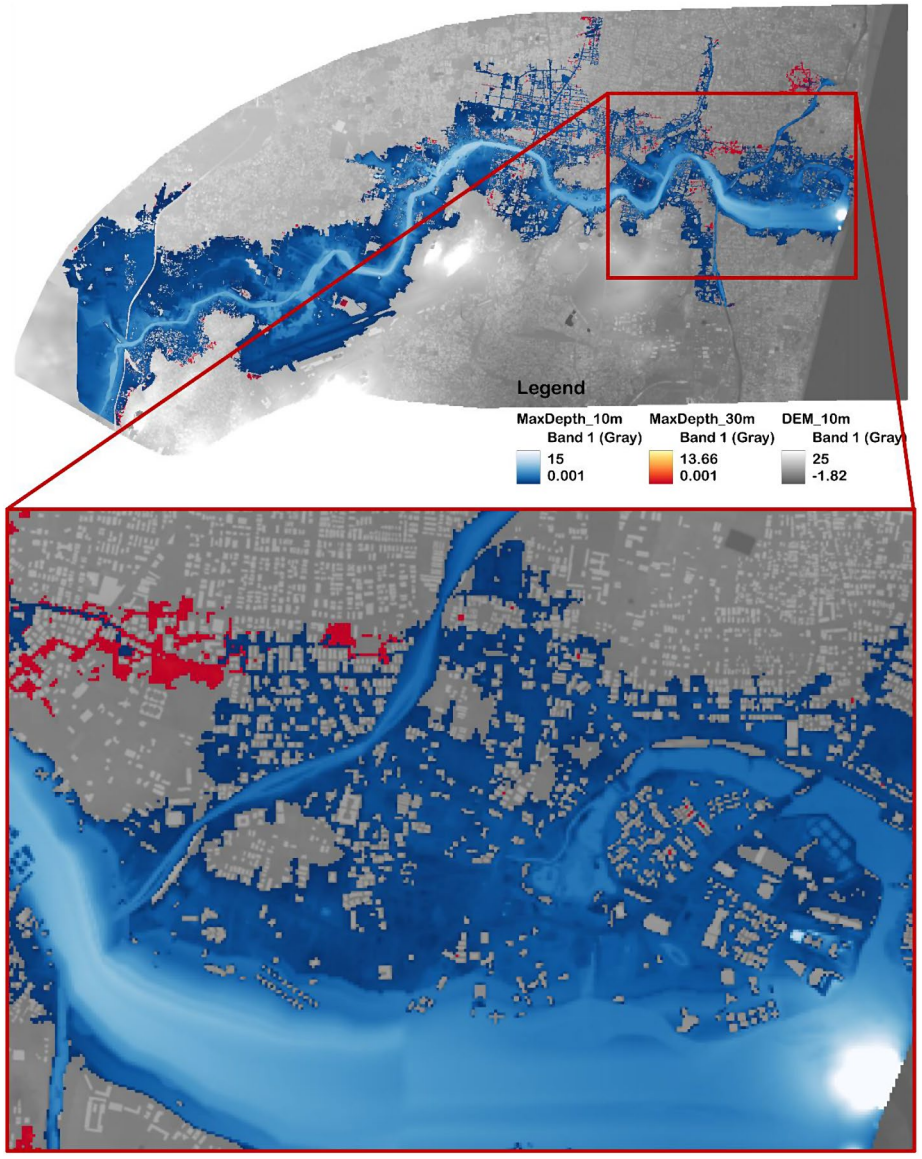

Fig. 19 Maximum inundation extent map for sub-grid simulations - Chennai

4.3.6 Comparison of computation time

The net computation time required for each run is given in Table 12. Similar to the Toce and Carlisle events, adopting the sub-grid approach reduces the run time considerably in this case as well - from days to minutes. The net computation time for the RM-3 model is 17,23,226 s. The sub-grid models 20 and 30 m produce similar accuracy as that of the RM-3

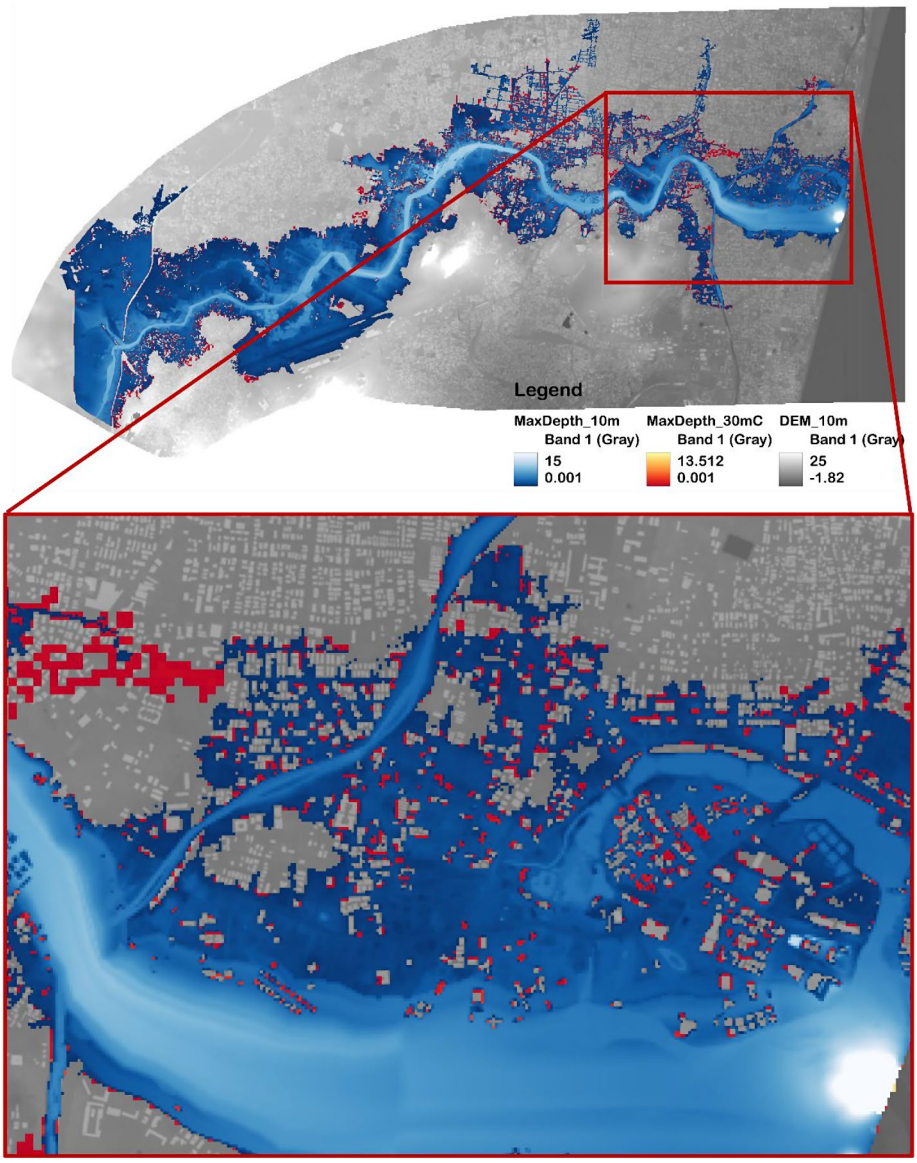

Fig. 20 Maximum inundation extent map for non-sub-grid simulations - Chennai

Table 10 Fitness Index: Chennai flood 2015

	Sub-grid models					Non-sub-grid models				
Grid size (m)	20	30	40	60	90	20	30	40	60	90
Fitness Index (%)	**98.4**	**97.6**	93.3	82.5	79.6	87.7	84.0	80.8	76.3	72.9

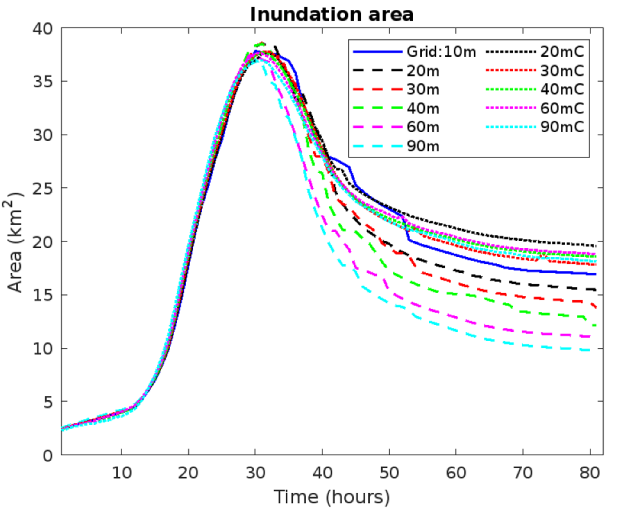

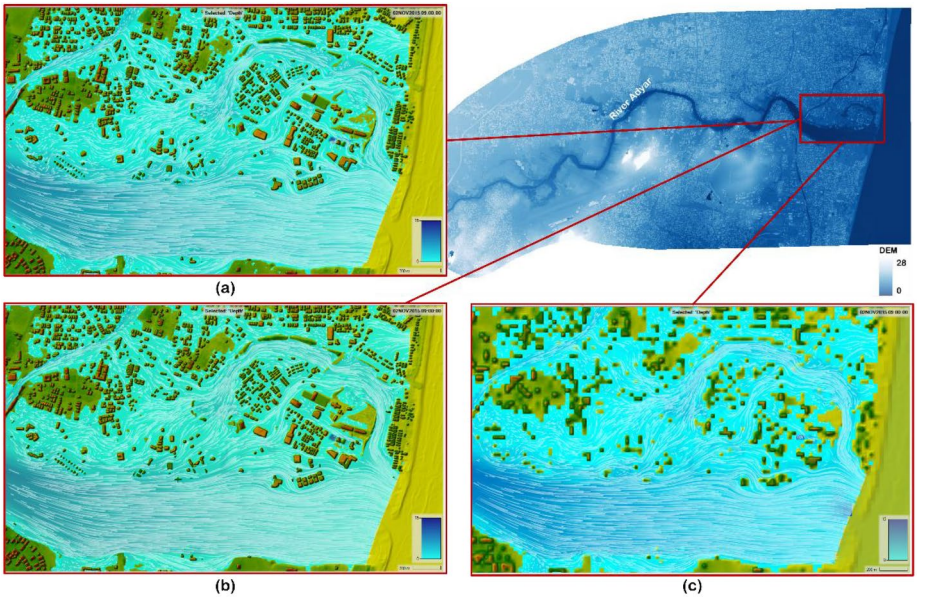

Fig. 21 Inundation area time-series graph for different grid sizes (sub-grid and non-sub-grid) – Chennai

Fig. 22 Velocity vectors around the urban features in R. A. Puram for: (a) RM-3, (b) 30 m sub-grid model, and (c) 30 m non-sub-grid model

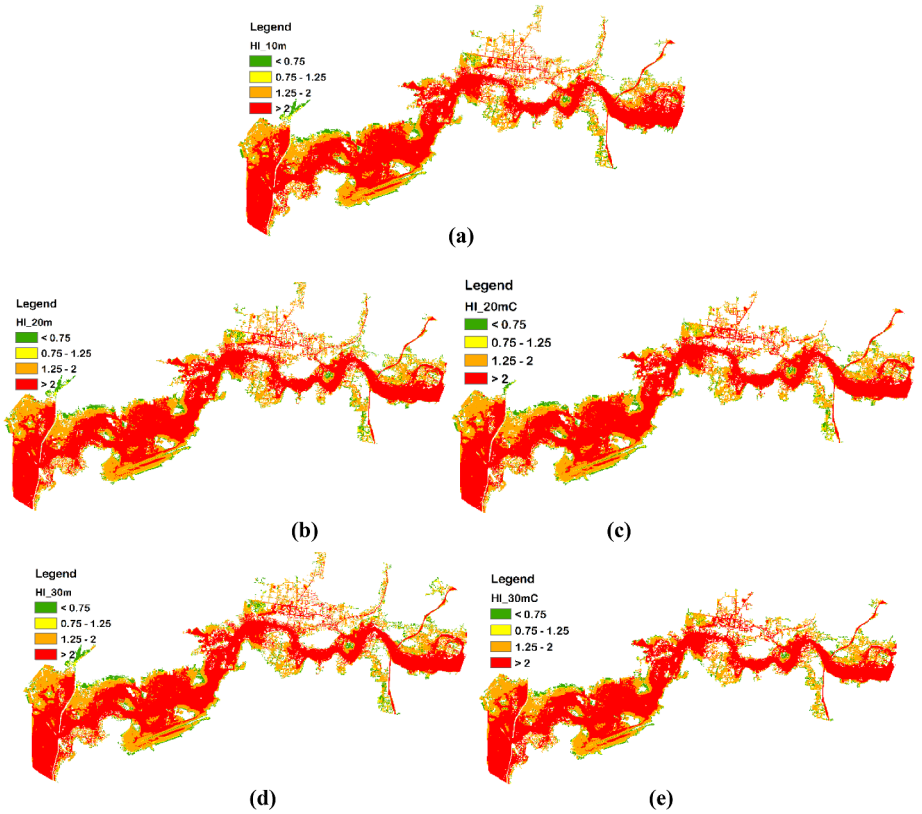

Fig. 23 Flood hazard maps of Chennai for: (a) RM-3, (b) 20 m sub-grid, (c) 20 m non-sub-grid (d) 30 m sub-grid, and (e) 30 m non-sub-grid models

Table 11 Area under each hazard zone for Adyar

Grid size (m)	Area under each hazard zone (sq. km)							
	Very low hazard		Danger for some		Danger for most		Danger for all	
	Sub-grid	Non-sub-grid	Sub-grid	Non-sub-grid	Sub-grid	Non-sub-grid	Sub-grid	Non-sub-grid
10	2.91		1.7		11.87		24.17	
20	2.99	2.55	1.69	1.67	12.17	11.64	23.27	
30	3.27	2.59	1.73	1.60	12.09	11.55	23.80	
40	3.18	2.47	1.64	1.49	12.04	11.29	23.98	
60	3.65	2.83	1.62	1.56	11.62	11.47	23.60	
90	3.81	3.08	1.53	1.60	10.99	11.07	23.55	

model in terms of simulation of inundation depth, inundation area, and flood risk levels at around 0.128 and 0.032 times the computational time consumed by RM-3.

Thus, computational efficiency, along with an accurate representation of urban flood scenarios, make the sub-grid model of 30 m best-suited for the simulation of real-time urban flood events in Chennai city when using a 10 m resolution DEM.

5 Conclusions

Computational time and accuracy in representing the complex urban topography are crucial in natural hazard analysis and formulating efficient disaster management and mitigation measures. The primary objective of this study was to establish the advantages and aptness of using the sub-grid approach for urban flood modeling and risk analysis. Urban flood simulations of the Toce Valley experimental test case, the Carlisle flood of 2005, and the Chennai flood of 2015 are performed using sub-grid and non-sub-grid approaches in the freely available HEC RAS 6.1.0 software package. Major conclusions drawn from the study are:

- **Inundation depth**: In terms of maximum inundation depths, the sub-grid model with coarser computational mesh and finer topographical description performed similarly to that of the reference model. Whereas the corresponding non-sub-grid model setups showed appreciable differences in all the cases. Based on the time evolution of inundation depth, it can be said that the flow amid the buildings, in the streets, and in the smaller canals in the corresponding test cases are simulated in a more or less similar accuracy by both optimal sub-grid setup and the reference model in all the cases. In contrast, the non-sub-grid model at coarser resolutions than the corresponding reference full 2D model fails to simulate the flood inundation depths accurately, especially in the urbanized flood plains. Thus, the ability to capture the underlying high-resolution terrain data along with the overlying coarse-resolution computational mesh details makes the sub-grid approach advantageous in terms of computational time and efficiency.
- **Inundation extent**: The fitness index for smaller sub-grid models (20 units and 30 units) are above 95% when compared respectively to the RM-1, RM-2, and RM-3 models (Toce, Carlisle, and Chennai flood scenarios, respectively), establishing their suitability in accurate urban flood simulations. Besides, for the real-time flood events of Carlisle and Chennai cities, the 30 m sub-grid is considered the best alternative owing to its lesser computation time involved in comparison with the 20 m sub-grid model. As expected, the non-sub-grid models of 20 and 30 m, respectively, reported 10% and 14% lesser fitness index values than the corresponding sub-grid models.
- **Flood risk mapping**: The 20 and 30 m sub-grid models can also capture the velocity

Table 12 Total computation time for each grid size

Grid size (m)	Total run time (hh:mm:ss)		Total run time (s)		Relative run time with respect to RM-2	
	Sub-grid	Non-sub-grid	Sub-grid	Non-sub-grid	Sub-grid	Non-sub-grid
20	61:10:53	59:11:02	220,253	213,062	0.1278	0.1236
30	15:04:17	12:34:35	54,257	45,275	0.0315	0.0263
40	06:19:13	04:46:48	22,753	17,208	0.0132	0.0099
60	03:10:22	01:33:04	11,422	5584	0.0066	0.0032
90	00:32:01	00:21:17	1921	1277	0.0011	0.0007

field similar to the reference model in both the real flood event simulations. Therefore, the areas under different flood risk levels are also accurately simulated by the 20 and 30 m sub-grid models for both events, thus rendering reliable flood hazard maps.

- **Computational cost**: The sub-grid model, at the optimal grid size of 20 mm- for Toce and 30 m for both the real flood events, simulates the urban flood dynamics significantly faster (~ 37, 85, and 32 times, respectively, for the considered case studies) than the high-resolution grid size reference models in the presented case studies without compromising accuracy. However, a site-specific trial is required to find an optimal combination of sub-grid resolution for terrain and numerical grid resolution for flux computation for acceptable accuracy and computation time.

Thus, the use of the sub-grid approach enables real-time urban flood forecast simulations and inundation mapping with better accuracy (time evolution of inundation depth and area, flood hazard maps) and lesser computation time than the traditional high-resolution flood simulations. In other words, the sub-grid approach examined herewith is particularly useful in the simulation of floods in urbanized flood plains with several smaller topographic features that govern the flood dynamics. A greater understanding of our results can be of use in the timely simulation of urban floods more accurately and reliably, enabling systematic and improved hazard analysis and flood damage mitigation, risk and hazard reduction, as well as preparedness.

Acknowledgements The authors are thankful to Paul D. Bates, Professor of Hydrology, School of Geographical Sciences, Cabot Institute for the Environment, for providing the necessary DEM, flow, and flood data of the Carlisle 2005 flood event required for the current work.
Statements and declarations.

Author contributions R. Reshma: Conceptualization; Data curation; Formal analysis; Methodology; Visualization; Writing - Original draft preparation & editing. N. Nithila Devi: Methodology, Writing - review & editing. Soumendra Nath Kuiry: Funding acquisition; Supervision; Resources, Writing - review & editing.

Funding This work was supported by Ministry of Electronics & Information Technology, the Government of India, under the project entitled *Urban modeling: Development of multi-sectorial simulation lab and science-based decision support framework to address urban environment issues* (Sanction Number: MeitY/R&D/HPC/2(1)/2014).

Declarations

Competing interests The authors have no relevant financial or non-financial interests to disclose.

References

Bates P, De Roo AP (2000) A simple raster-based model for flood inundation simulation. J Hydrol 236(1–2):54–77. https://doi.org/10.1016/S0022-1694(00)00278-X

Bates PD, Wilson MD, Horritt MS, Mason DC, Holden N, Currie A (2006) Reach scale floodplain inundation dynamics observed using airborne synthetic aperture radar imagery: data analysis and modelling. J Hydrol 328(1–2):306–318. https://doi.org/10.1016/j.jhydrol.2005.12.028

Bates PD, Horritt MS, Fewtrell TJ (2010) A simple inertial formulation of the shallow water equations for efficient two-dimensional flood inundation modelling. J Hydrol 387(1–2):33–45. https://doi.org/10.1016/j.jhydrol.2010.03.027

Beffa C, Connell RJ (2001) Two-Dimensional Flood Plain Flow. I: model description. J Hydrol Eng 6(5):397–405. https://doi.org/10.1061/(ASCE)1084-0699(2001)6:5(397)
Berger MJ, Colella P (1989) Local adaptive mesh refinement for shock hydrodynamics. J Comput Phys 82(1):64–84. https://doi.org/10.1016/0021-9991(89)90035-1
Brett F, Sanders M (2001) High-resolution and non-oscillatory solution of the St. Venant equations in non-rectangular and non-prismatic channels. J Hydraul Res 39(3):321–330. https://doi.org/10.1080/00221680109499835
Chang T-J, Yu H-L, Wang C-H, Chen AS (2022) Dynamic-wave cellular automata framework for shallow water flow modeling. J Hydrol 613:128449. https://doi.org/10.1016/j.jhydrol.2022.128449
Chen AS, Evans B, Djordjević S, Savić DA (2012) A coarse-grid approach to representing building blockage effects in 2D urban flood modelling. J Hydrol 426–427:1–16. https://doi.org/10.1016/j.jhydrol.2012.01.007
Courty LG, Pedrozo-Acuña A, Bates PD (2017) Itzï (version 17.1): an open-source, distributed GIS model for dynamic flood simulation. Geosci Model Dev 10(4):1835–1847. https://doi.org/10.5194/gmd-10-1835-2017
EM-DAT | The international disasters database. (2023) https://public.emdat.be/
Fernández-Pato J, García-Navarro P (2021) An efficient GPU implementation of a coupled overland-sewer hydraulic model with Pollutant Transport. Hydrology 8(4):146. https://doi.org/10.3390/hydrology8040146
Glaister P (1988) Approximate Riemann solutions of the shallow water equations. J Hydraul Res 26(3):293–306. https://doi.org/10.1080/00221688809499213
Guinot V, Soares-Frazão S (2006) Flux and source term discretization in two-dimensional shallow water models with porosity on unstructured grids. Int J Numer Methods Fluids 50(3):309–345. https://doi.org/10.1002/fld.1059
Gupta AK, Nair S (2010) Flood risk and context of land-uses: Chennai city case. J Geogr Reg Plann 3(12):365–372. https://academicjournals.org/journal/JGRP/article-full-text-pdf/18C62DC40738.pdf
Haltas I, Elçi S, Tayfur G (2016) Numerical Simulation of Flood Wave Propagation in two-dimensions in densely populated urban areas due to dam break. Water Resour Manage 30(15):5699–5721. https://doi.org/10.1007/S11269-016-1344-4
Haltas I, Tayfur G, Elci S (2016b) Two-dimensional numerical modeling of flood wave propagation in an urban area due to Ürkmez dam-break, İzmir, Turkey. Nat Hazards 81(3):2103–2119. https://doi.org/10.1007/S11069-016-2175-6
HEC-RAS River Analysis System Hydraulic Reference Manual. (2016) www.hec.usace.army.mil
Hosseiny H, Nazari F, Smith V, Nataraj C (2020) A Framework for modeling Flood depth using a hybrid of Hydraulics and Machine Learning. Sci Rep 10(1):8222. https://doi.org/10.1038/s41598-020-65232-5
Hou J, Zhou N, Chen G, Huang M, Bai G (2021) Rapid forecasting of urban flood inundation using multiple machine learning models. Nat Hazards 108(2):2335–2356. https://doi.org/10.1007/S11069-021-04782-X
Hu R, Fang F, Salinas P, Pain CC (2018) Unstructured mesh adaptivity for urban flooding modelling. J Hydrol 560:354–363. https://doi.org/10.1016/j.jhydrol.2018.02.078
Hunt J (2009) *Appendix H-Flood Hazard Information*. http://randd.defra.gov.uk/Document.aspx?Document=FD2321_7400_PR.pdf
Köppen climate classification Encyclopedia Britannica - Google Search. (n.d.). In *Earth and Space Science*
Kuiry SN, Sen D, Bates PD (2010) Coupled 1D–Quasi-2D Flood Inundation Model with unstructured grids. J Hydraul Eng 136(8):493–506. https://doi.org/10.1061/(ASCE)HY.1943-7900.0000211
Kwon SH, Kim JH (2021) Machine Learning and Urban Drainage Systems: State-of-the-art review. Water 13(24):3545. https://doi.org/10.3390/w13243545
Li B, Phillips M, A. Fleming C (2006) Application of 3D hydrodynamic model to flood risk assessment. Proc Inst Civil Eng Water Manag 159(1):63–75. https://doi.org/10.1680/WAMA.2006.159.1.63/ASSET/IMAGES/SMALL/WAMA159-063-F21.GIF
Li L, Mei, Shao W, Yan (2019) Comparative analysis of building representations in TELEMAC-2D for Flood Inundation in Idealized Urban districts. Water 11(9):1840. https://doi.org/10.3390/w11091840
Liu Y, Pender G (2013) Carlisle 2005 urban flood event simulation using cellular automata-based rapid flood spreading model. Soft Comput 17(1):29–37. https://doi.org/10.1007/s00500-012-0898-1
McMillan HK, Brasington J (2007) Reduced complexity strategies for modelling urban floodplain inundation. Geomorphology 90(3–4):226–243. https://doi.org/10.1016/j.geomorph.2006.10.031
Mignot E, Dewals B (2022) Hydraulic modelling of inland urban flooding: recent advances. J Hydrol 127763. https://doi.org/10.1016/j.jhydrol.2022.127763
Mignot E, Li X, Dewals B (2019) Experimental modelling of urban flooding: a review. J Hydrol 568:334–342. https://doi.org/10.1016/j.jhydrol.2018.11.001

Mohanty MP, Mudgil S, Karmakar S (2020) Flood management in India: a focussed review on the current status and future challenges. Int J Disaster Risk Reduct 49:101660. https://doi.org/10.1016/J.IJDRR.2020.101660

Muhadi NA, Abdullah AF, Bejo SK, Mahadi MR, Mijic A (2020) The Use of LiDAR-Derived DEM in Flood applications: a review. Remote Sens 12(14):2308. https://doi.org/10.3390/rs12142308

Mustafa A, Szydłowski M (2021) Application of different building representation techniques in HEC-RAS 2-D for urban flood modeling using the Toce River experimental case. PeerJ 9. https://doi.org/10.7717/peerj.11667

Muthusamy M, Casado MR, Butler D, Leinster P (2021) Understanding the effects of Digital Elevation Model resolution in urban fluvial flood modelling. J Hydrol 596:126088. https://doi.org/10.1016/j.jhydrol.2021.126088

Narasimhan B, Bhallamudi SM, Mondal A, Ghosh S, Mujumdar P (2016) *Chennai floods 2015 - A Rapid Assessment*. https://www.almendron.com/tribuna/wp-content/uploads/2017/03/chennai-floods-rapid-assessment-report-may-23-2016.pdf

Neal JC, Bates PD, Fewtrell TJ, Hunter NM, Wilson MD, Horritt MS (2009) Distributed whole city water level measurements from the Carlisle 2005 urban flood event and comparison with hydraulic model simulations. J Hydrol 368(1–4):42–55. https://doi.org/10.1016/j.jhydrol.2009.01.026

Neal JC, Fewtrell TJ, Bates PD, Wright NG (2010) A comparison of three parallelisation methods for 2D flood inundation models. Environ Model Softw 25(4):398–411. https://doi.org/10.1016/j.envsoft.2009.11.007

Nithila Devi N, Sridharan B, Kuiry SN (2019) Impact of urban sprawl on future flooding in Chennai city, India. J Hydrol 574:486–496. https://doi.org/10.1016/j.jhydrol.2019.04.041

Nithila Devi N, Sridharan B, Bindhu VM, Narasimhan B, Bhallamudi SM, Bhatt CM, Usha T, Vasan DT, Kuiry SN (2020) Investigation of role of Retention Storage in tanks (Small Water bodies) on future urban flooding: a case study of Chennai City, India. Water 12(10):2875. https://doi.org/10.3390/w12102875

Nkeki FN, Bello EI, Agbaje IG (2022) Flood risk mapping and urban infrastructural susceptibility assessment using a GIS and analytic hierarchical raster fusion approach in the Ona River Basin, Nigeria. Int J Disaster Risk Reduct 77:103097. https://doi.org/10.1016/J.IJDRR.2022.103097

Prestininzi P (2008) Suitability of the diffusive model for dam break simulation: application to a CADAM experiment. J Hydrol 361(1–2):172–185. https://doi.org/10.1016/j.jhydrol.2008.07.050

Sanders BF, Schubert JE, Gallegos HA (2008) Integral formulation of shallow-water equations with anisotropic porosity for urban flood modeling. J Hydrol 362(1–2):19–38. https://doi.org/10.1016/j.jhydrol.2008.08.009

Schubert JE, Sanders BF (2012) Building treatments for urban flood inundation models and implications for predictive skill and modeling efficiency. Adv Water Resour 41:49–64. https://doi.org/10.1016/j.advwatres.2012.02.012

Shustikova I, Domeneghetti A, Neal JC, Bates P, Castellarin A (2019) Comparing 2D capabilities of HEC-RAS and LISFLOOD-FP on complex topography. Hydrol Sci J 64(14):1769–1782. https://doi.org/10.1080/02626667.2019.1671982

Sridharan B, Gurivindapalli D, Kuiry SN, Mali VK, Devi N, Bates N, P. D., Sen D (2020) Explicit expression of Weighting Factor for Improved Estimation of Numerical Flux in local Inertial models. Water Resour Res 56(7). https://doi.org/10.1029/2020WR027357

Sridharan B, Bates PD, Sen D, Kuiry SN (2021) Local-inertial shallow water model on unstructured triangular grids. *Advances in Water Resources*, *152*. https://doi.org/10.1016/j.advwatres.2021.103930

Surendran S, Gibbs G, Wade S, Udale-Clarke H, Wallingford HR (2008) Supplementary Note on Flood Hazard Ratings and Thresholds for Development Planning and Control Purpose—Clarification of the Table 13.1 of FD2320/TR2. In *assets.publishing.service.gov.uk*. https://assets.publishing.service.gov.uk/media/602bbdcfe90e070561b31432/Explanatory_note_for_FD2320_and_FD2321_project_record.pdf

Testa G, Zuccalà D, Alcrudo F, Mulet J, Soares-Frazão S (2007a) Flash flood flow experiment in a simplified urban district. *Journal of Hydraulic Research*, *45*(SPEC. ISS.), 37–44. https://doi.org/10.1080/00221686.2007.9521831

Testa G, Zuccalà D, Alcrudo F, Mulet J, Soares-Frazão S (2007b) Flash flood flow experiment in a simplified urban district. *Taylor & Francis*, *45*(SPEC. ISS.), 37–44. https://doi.org/10.1080/00221686.2007.9521831

UNDRR (2009) *UNISDR terminology on disaster risk reduction*. https://www.undrr.org/publication/2009-unisdr-terminology-disaster-risk-reduction

Xing Y, Liang Q, Wang G, Ming X, Xia X (2019) City-scale hydrodynamic modelling of urban flash floods: the issues of scale and resolution. Nat Hazards 96(1):473–496. https://doi.org/10.1007/S11069-018-3553-Z/FIGURES/19

Yan X, Xu K, Feng W, Chen J (2021) A Rapid Prediction Model of Urban Flood Inundation in a high-risk area Coupling Machine Learning and Numerical Simulation approaches. Int J Disaster Risk Sci 12(6):903–918. https://doi.org/10.1007/s13753-021-00384-0